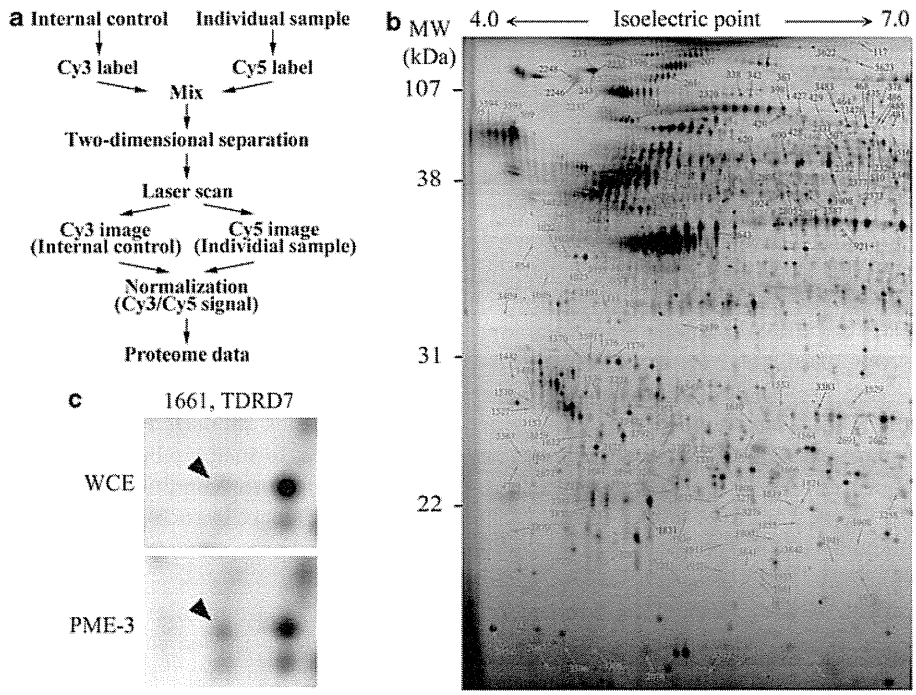

Figure 2 Protein expression profiling by two-dimensional difference gel electrophoresis (2D-DIGE). Schematic diagram of work flow of 2D-DIGE (**a**). Image of separated proteins on the gel. Enlarged 2D image is shown in Supplementary Figure 1A (**b**). The location of protein spots for TDRD7 was observed in pseudopodia (upper) and whole-cell (lower) lysates (**c**).

discovery rate of <0.001, and a fold difference of >6 between the protrusions and the whole cell group; spots for 3 μm pore membrane group, a false discovery rate of <0.001, and a fold difference of >4 between the protrusions of the 3 μm porous membrane group and the whole cell group. According to these criteria, we selected 67 and 132 spots with higher intensity and 29 and 74 spots with lower intensity in PME for the 1 μm porous membrane (PME-1) and PME for the 3 μm porous membrane (PME-3) than in WCE, respectively (Table 1). Protein identification using liquid chromatography-mass spectrometry/mass spectrometry (LC-MS/MS) revealed 21 and 45 unique proteins with higher expression in PME-1 and PME-3 than in the WCE, and 19 and 36 proteins with lower expression in PME-1 and PME-3, respectively (Table 1, Supplementary Tables S1–S3; all supportive data for protein identification, including raw data, are available upon request). The representative mass spectrum is shown in Supplementary Figure S3. All but two proteins were commonly enriched or lowered in PME-1 and PME-3. As an example of proteins in the pseudopodia fraction, the localization of TDRD7 (spot number 1661) is demonstrated in Figure 2c.

Subcellular Localization of Identified Proteins

Localization of the identified proteins was immunohistochemically validated using antibodies against RAB1A, HSP90B, TDRD7, and vimentin. First, we examined subcellular localization of these proteins in MDA-MB-231 cells without treatment using NIH3T3-conditioned medium. The four proteins showed unique localizations: RAB1A, diffuse pattern in the nucleus and cytoplasm (Figure 3); HSP90B, mesh-like or punctate appearance in the cytoplasm; TDRD7, spotty features in the nucleus; and vimentin, cytoskeletal fibrous structures (Figures 4–6, respectively). Phalloidin staining demonstrated well-developed actin stress fibers across cells. No pseudopodial microprocesses were observed when NIH3T3-conditioned medium was not used. After treatment with NIH3T3-conditioned medium, pseudopodial microprocesses were observed and these proteins localized in pseudopodial microprocesses with actin stress fibers at the cell-membrane interface. Immunohistochemical analysis confirmed a novel localization of RAB1A, HSP90B, TDRD7, and vimentin in pseudopodial microprocesses, which is consistent with the results of 2D-DIGE (Table 1 and Figures 3–6). In addition, endogenous RAB1A, HSP90B, TDRD7, and vimentin expression for naive MDA-MB-231 cells, human lung tissue, and human lung adenocarcinoma A549 cells was validated using western blot (Supplementary Figure S4).

The Length of Pseudopodial Microprocesses

To validate whether the identified molecules are involved in forming pseudopodial microprocesses, RAB1A over-

Table 1 Proteins upregulated in pseudopodia microprocesses in 1 or 3 μm porous membrane

Accession no.	Identified protein[a]
Cytoskeleton (3)	
Actin-associated (2)	
P60709	Actin, cytoplasmic 1
P04632	Calpain small subunit 1
Intermediate filament (1)	
P08670	Vimentin
Chaperones (5)	
P08238	Heat shock protein HSP 90-β
P11142	Heat shock cognate 71 kDa protein
P40227	T-complex protein 1 subunit-æ
Q9UHV9	Prefoldin subunit 2
Translation (2)	
P60842	Eukaryotic initiation factor 4A-I
P08865	40S ribosomal protein SA
Q13765	Nascent polypeptide-associated complex subunit-α
RNA binding proteins (1)	
O00571	ATP-dependent RNA helicase DDX3X
Ub/Proteasome (1)	
Q99460	26S proteasome non-ATPase regulatory subunit 1
Signaling (7)	
P61981	14-3-3 protein γ
P52565	Rho GDP-dissociation inhibitor 1
P81605	Dermcidin
Q92734	Protein TFG
Q13795	ADP-ribosylation factor-related protein 1
P01024	Complement C3
P54756	Ephrin type-A receptor 5
Trafficking (4)	
P48444	Coatomer subunit δ
P62820	Ras-related protein Rab-1A
P20340	Ras-related protein Rab-6A
Q9BY43	Charged multivesicular body protein 4a
Organelles (9)	
Endoplasmic reticulum (2)	
P11021	78 kDa glucose-regulated protein
Q01105	Protein SET
Nucleus (6)	
P45973	Chromobox protein homolog 5
P06748	Nucleophosmin
P60174	Triosephosphate isomerase
Q12905	Interleukin enhancer-binding factor 2
Q9UNZ2	NSFL1 cofactor p47
Q99733	Nucleosome assembly protein 1-like 4
Q56NI9	N-acetyltransferase ESCO2
Q9BS16	Centromere protein K
Others (13)	
P08758	Annexin A5
P02792	Ferritin light chain
Q15181	Inorganic pyrophosphatase
P09211	Glutathione *S*-transferase P
O95394	Phosphoacetylglucosamine mutase
O75223	γ-Glutamylcyclotransferase
P07741	Adenine phosphoribosyltransferase
P50452	Serpin B8
Q9NS25	Sperm protein associated with the nucleus on the X chromosome B/F
Q9P1Z9	Uncharacterized protein KIAA1529 (also known as TDRD7)
Q9H0J4	Glutamine-rich protein 2
Q9NQ48	Leucine zipper transcription factor-like protein 1
Q8IUR5	Transmembrane and TPR repeat-containing protein 1

TDRD7, tudor domain containing 7.
The numeric character in the parentheses means the numbers of identified proteins for each group.
[a]Protein list, supportive information for protein identification, and functional classification are detailed in Supplementary Tables.

expression and knockdown experiments were conducted on MDA-MB-231 cells on the 3 μm porous membrane with the conditioned medium followed by western blotting. We subcloned the RAB1A cDNA into the mammalian expression vector, pCX4-bsr and the RAB1A-targetting siRNA into pSilencer4.1-CMVneo. Western blot analyses revealed that MDA-MB-231 cells overexpressed RAB1A when the cells were transfected with RAB1A cDNA plasmid, whereas RAB1A expression was faint with RAB1A-targetting siRNA (Supplementary Figure S5a). Moreover, the longer pseudopodial microprocesses with phalloidin staining were observed in the RAB1A-overexpressed cells and the fewer and shorter microprocesses were in the RAB1A-knockdown cells compared with the nontransfected cells using confocal microscopy (Supplementary Figure S5b and c).

DISCUSSION

Identification of proteins associated with psuedopodia structure and functions will lead to a further understanding of cell migration. Tumor cell migration is involved in a critical part of invasion and metastasis. Therefore, such proteins for tumor cells can be considered as a candidate of molecular biomarkers and therapeutic targets. We demonstrated that the combined use of the medical laser technology

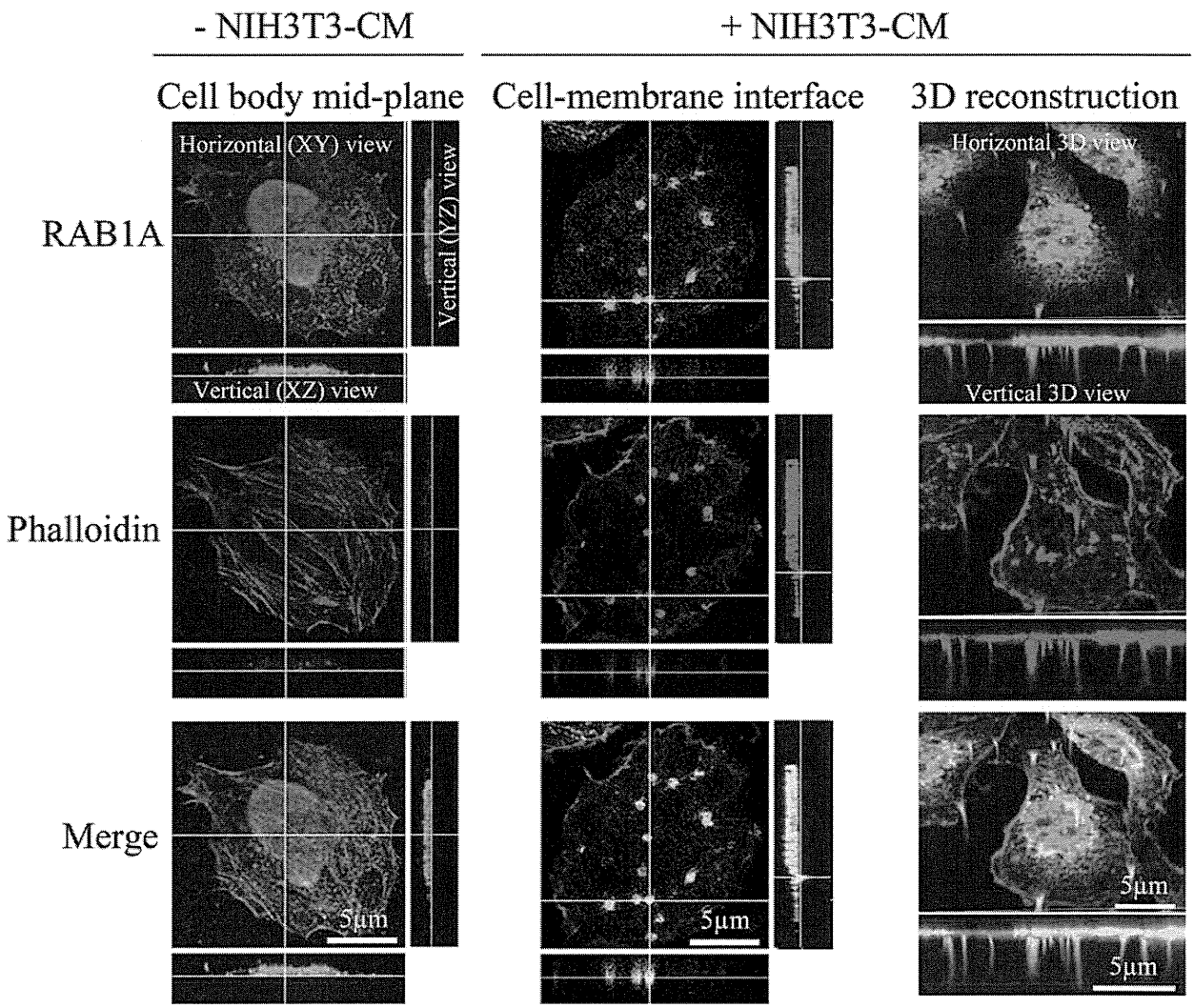

Figure 3 Immunohistochemical view of RAB1A in pseudopodia. Localization of RAB1B before and after treatment with NIH3T3-conditioned medium was determined using immunohistochemical staining. Phalloidin staining was performed to visualize F-actin as a control in pseudopodial microprocesses. Note that RAB1A was observed as a dot-like structure in the horizontal view and as a protrusion in the vertical view following stimulation by NIH3T3-conditioned medium. RAB1A colocalized with F-actin after treatment and was detectable throughout the microprocess.

and the highly sensitive proteomics modalities identified a scarce amount of pseudopodia proteins.

When the cell body was removed by an excimer laser-assisted cell etching technique, there was no obvious damage on the pseudopodia appearances (Figure 1c) and the proteins in the pseudopodia remained intact (Figure 1d). This observation is supported by photochemistry and photophysics backgrounds. The laser keratectomy system used in this study was equipped with an argon fluoride excimer laser with a wavelength of 193 nm. Absorption at this wavelength is due primarily to peptide bonds (O = CNN) in the backbone of proteins in the cell rather than to water. Moreover, the optical absorption depth of the cell at 190 nm is estimated to be $\sim$500 nm.[20] This suggests that protein degradation can be induced only within a depth of 500 nm from the base of the pseudopodia. Additionally, pore size of the porous membrane (1 or 3 μm) is small relative to the excimer laser wavelength, that is, $\leq$15.5 times as large as the wavelength (193 nm). This causes the membrane to exhibit a strong light-scattering effect at a wavelength of 193 nm. As a consequence, the excimer laser pulses cannot penetrate into the pores. With these backgrounds and experimental observations, we concluded that the excimer laser ablation did not cause significant protein degradation in the pseudopodia.

Using 2D-DIGE and high sensitive fluorescent dye, we can perform global protein expression studies. Indeed, only a few micrograms of proteins were enough to investigate the psuedopodia-associated proteins in this study. However,

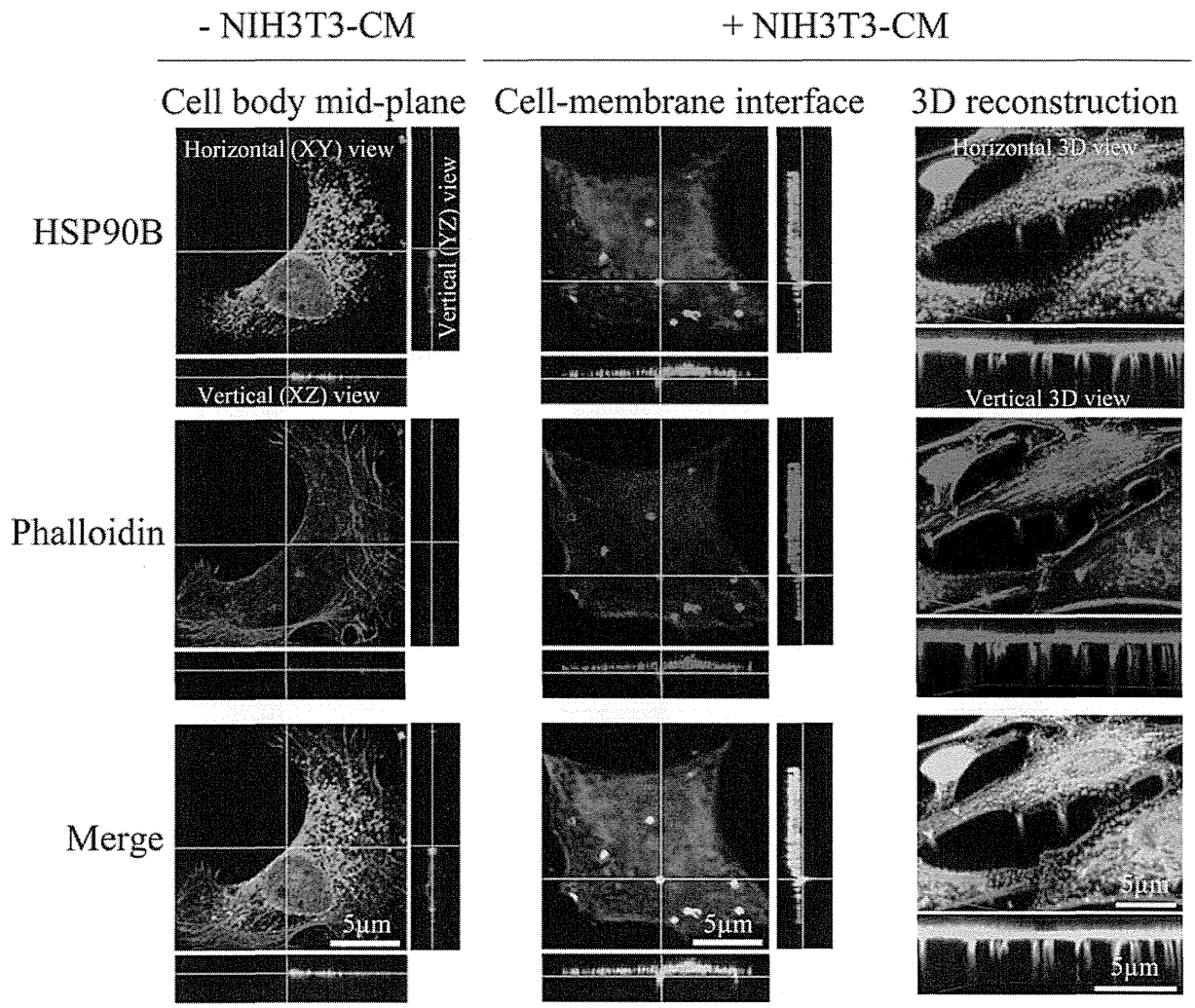

Figure 4 Immunohistochemical view of HSP90B in pseudopodia. Localization of HSP90B without and with treatment with NIH3T3-conditioned medium was determined using immunohistochemical staining. Phalloidin staining was performed to visualize F-actin as a control protein in pseudopodial microprocesses. Note that HSP90B was observed as dot-like structures in the horizontal view and as protrusions in the vertical view after stimulation using NIH3T3-conditioned medium. HSP90B colocalized with F-actin after treatment and was detectable throughout the microprocess.

2D-DIGE allows observation of the proteins with middle to high expression level. This is because of the fact that 2D-DIGE does not select the proteins, and the proteins are detected in the order of expression level. In the case of mass spectrometry-based proteomics, several hundred micrograms of proteins are required for quantitative protein expression profiling, and psuedopodia proteins may not be investigated in a quantitative way. In addition, mass spectrometry also visualizes proteins in the order of expression level, and proteins with low expression may not be observed. Antibody-based proteomics such as antibody array can achieve sensitive and quantitative expression study. We may be able to observe proteins of small amount such as receptors and kinases. However, antibody-based proteomics generally requires much amount of proteins, and cannot be applied for the study of pseudopodia proteins. Taken all together, we concluded that 2D-DIGE is a best method among the proteomics modalities for psuedopodia proteomics.

Among identified proteins, 12 highly expressed proteins in PME molecules, including cytoskeletal and chaperone proteins, were also identified in a past report involving pseudopodial proteomics.[4] This finding indicated that the present new method certainly examined pseudopodia. On the other hand, pseudopodia in the 1 μm pore may morphologically seem to be a part of that in the 3 μm pore. This speculation was supported by the observation that most identified molecules in PME-1 were observed in PME-3. The overlapped proteins may be most specific candidate molecules that lead or promote cell migration. On the other hand, several identified proteins, such as TDRD7 and

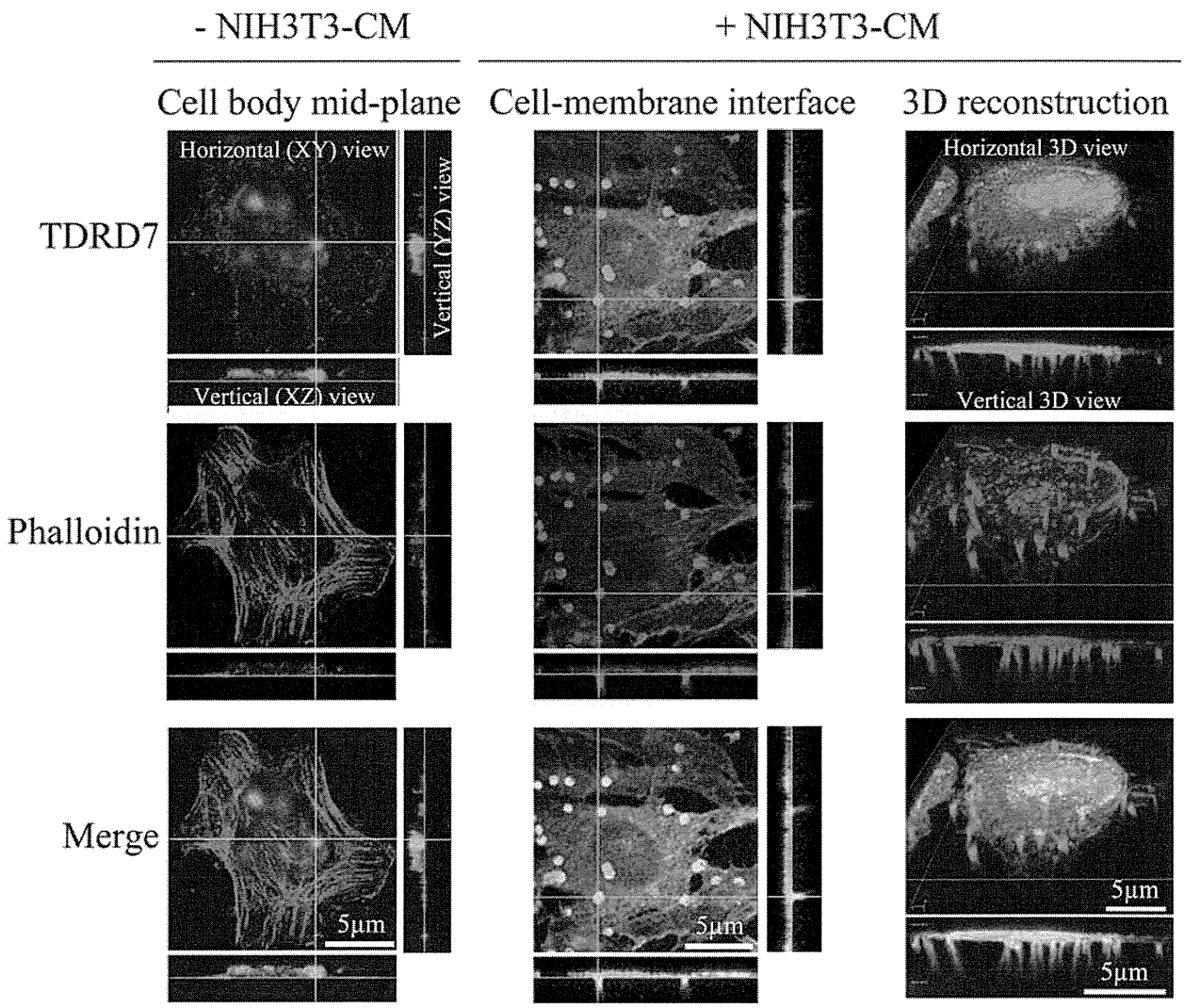

Figure 5 Immunohistochemical view of TDRD7 in pseudopodia. Localization of TDRD7 without and with treatment using NIH3T3-conditioned medium was determined using immunohistochemical staining. Phalloidin staining was performed to visualize F-actin as a control protein in pseudopodial microprocesses. Note that TDRD7 was observed as dot-like structures in the horizontal view and as protrusions in the vertical view after stimulation using NIH3T3-conditioned medium. TDRD7 colocalized with F-actin after treatment and was primarily located in the proximal region of the microprocess.

vimentin, were identified in both 'upregulated proteins' and 'downregulated proteins' in PME compared with WCE. One considerable reason is that specific forms of TDRD7 and vimentin are differently regulated between pseudopodia and cell body. The variations of protein spots may reflect the different posttranslational modifications, and they may play distinct roles in cell behaviors. Further characterization of their posttranslational modifications in relation to psuedopodia should be an interesting subject, although it is not easy because of the sensitivity of mass spectrometry and a lack of methods to control the expression of specific protein forms.

In the present study, the localization of RAB1A, HSP90B, TDRD7, and vimentin in the pseudopodia with actin stress fiber, which is known to be enriched in pseudopodia,[1,2] was confirmed by immunohistochemical experiment (Figures 3–6). In addition, RAB1A was indicated to play an important role in forming and extending pseudopodial microprocesses in human breast cancer cells by overexpression and knockdown experiments. Previous studies demonstrated that these four proteins may function in the process of cell migration. HSP90B is known to function as a chaperone for proper folding of integrin molecules.[21,22] Vimentin filaments are shown to be connected to integrin matrix adhesion sites.[23] Interestingly, guanosine triphosphatase activity of RAB1A and N-terminal phosphorylation of vimentin filaments are involved in vesicle trafficking of integrins to the plasma membrane.[24] Although the specific function is still unknown, TDRD7 is a scaffold for various proteins including

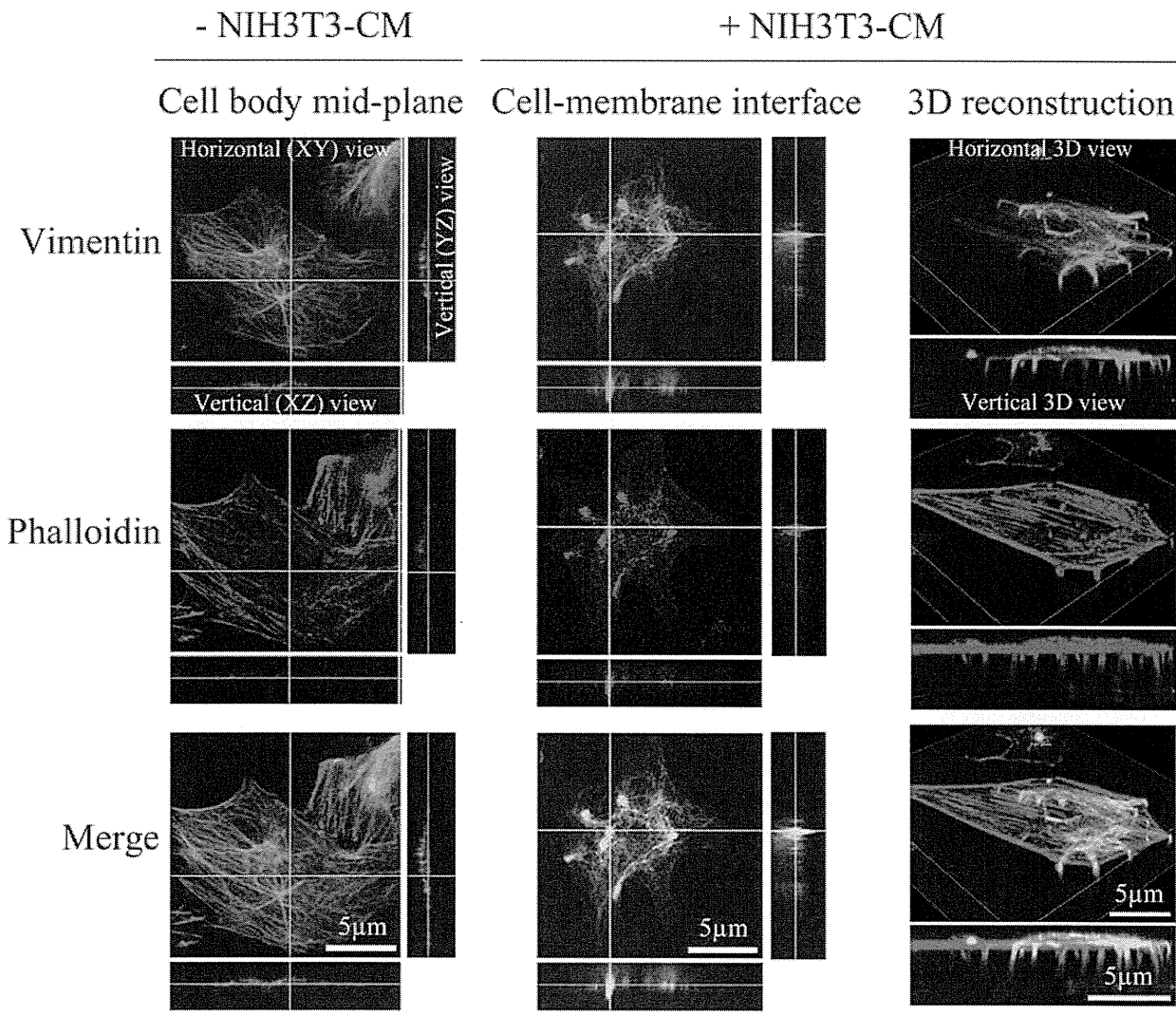

Figure 6 Immunohistochemical view of vimentin in pseudopodia. Localization of vimentin without and with treatment using NIH3T3-conditioned medium was determined using immunohistochemical staining. Phalloidin staining was performed to visualize F-actin as a control protein in pseudopodial microprocesses. Note that vimentin was observed as dot-like structures in the horizontal view and as protrusions in the vertical view after stimulation using NIH3T3-conditioned medium. Vimentin colocalized with F-actin after treatment and was primarily located in the proximal region of the microprocess.

Ser/Thr kinase PCTAIRE 2[25] and TACC1.[26] Thus, these four proteins may participate in integrin-dependent pseudopodia formation and directional cell migration. Their functional role for pseudopodia and possible clinical utilities are worth investigating in further studies.

In conclusion, we established a novel application for pseudopodia proteomics by using a fully developed medical nanodevice and a proteomic modality. Proteomics showed pseudopodia to be dynamic cellular components involved in cytoskeletal remodeling, protein synthesis, trafficking, and degradation as well as involved in various signal transduction pathways. We observed significant proteomic differences between pseudopodia of different diameters and between cell lines with different motile potentials. We confirmed novel pseudopodial localization of RAB1A, HSP90B, TDRD7, and vimentin, which play an important role in cell migration. Additional proteomic studies using varying pore sizes of membranes and different cell types, followed by functional studies of the identified proteins, will reveal the precise molecular basis of cell migration.

Supplementary Information accompanies the paper on the Laboratory Investigation website (http://www.laboratoryinvestigation.org)

ACKNOWLEDGEMENTS

This work was supported by grants from the Ministry of Education, Culture, Sports, Science and Technology of Japan, from the Nakatani Foundation of Electronic Measuring Technology Advancement, from the Ministry of Health, Labor and Welfare, and from the Program for Promotion of Fundamental Studies in Health Sciences of the Organization for Pharmaceutical Safety and Research of Japan.

DISCLOSURE/CONFLICT OF INTEREST

The authors declare no conflict of interest.

1. *Lauffenburger DA, Horwitz AF. Cell migration: a physically integrated* molecular process. Cell 1996;84:359–369.
2. Parent CA, Devreotes PN. A cell's sense of direction. Science 1999;284: 765–770.
3. Nguyen TN, Wang HJ, Zalzal S, *et al.* Purification and characterization of beta-actin-rich tumor cell pseudopodia: role of glycolysis. Exp Cell Res 2000;258:171–183.
4. Jia Z, Barbier L, Stuart H, *et al.* Tumor cell pseudopodial protrusions. Localized signaling domains coordinating cytoskeleton remodeling, cell adhesion, glycolysis, RNA translocation, and protein translation. J Biol Chem 2005;280:30564–30573.
5. Wang Y, Ding SJ, Wang W, *et al.* Profiling signaling polarity in chemotactic cells. Proc Natl Acad Sci USA 2007;104:8328–8333.
6. Wang Y, Ding SJ, Wang W, *et al.* Methods for pseudopodia purification and proteomic analysis. Sci STKE 2007;2007:pl4.
7. Reynolds A, Moore JE, Naroo SA, *et al.* Excimer laser surface ablation - a review. Clin Experiment Ophthalmol 2010;38:168–182.
8. Solomon KD, Fernandez de Castro LE, Sandoval HP, *et al.* LASIK world literature review: quality of life and patient satisfaction. Ophthalmology 2009;116:691–701.
9. Hanash S, Taguchi A. The grand challenge to decipher the cancer proteome. Nat Rev Cancer 2010;10:652–660.
10. Kondo T, Hirohashi S. Application of highly sensitive fluorescent dyes (CyDye DIGE Fluor saturation dyes) to laser microdissection and two-dimensional difference gel electrophoresis (2D-DIGE) for cancer proteomics. Nat Protoc 2007;1:2940–2956.
11. Kondo T, Seike M, Mori Y, *et al.* Application of sensitive fluorescent dyes in linkage of laser microdissection and two-dimensional gel electrophoresis as a cancer proteomic study tool. Proteomics 2003;3:1758–1766.
12. Shaw J, Rowlinson R, Nickson J, *et al.* Evaluation of saturation labelling two-dimensional difference gel electrophoresis fluorescent dyes. Proteomics 2003;3:1181–1195.
13. Unlu M, Morgan ME, Minden JS. Difference gel electrophoresis: a single gel method for detecting changes in protein extracts. Electrophoresis 1997;18:2071–2077.
14. Kondo T, Hirohashi S. Application of 2D-DIGE in cancer proteomics toward personalized medicine. Methods Mol Biol 2009;577:135–154.
15. Ito A, Kataoka TR, Watanabe M, *et al.* A truncated isoform of the PP2A B56 subunit promotes cell motility through paxillin phosphorylation. EMBO J 2000;19:562–571.
16. Du CX, Shen Y, Wang Y. Comparison of high order aberration after conventional and customized ablation in myopic LASIK in different eyes of the same patient. J Zhejiang Univ Sci B 2007;8:177–180.
17. Victor G, Urbano A, Marcal S, *et al.* [First Brazilian refractive surgery survey]. Arq Bras Oftalmol 2005;68:727–733.
18. Akagi T, Murata K, Shishido T, *et al.* v-Crk activates the phosphoinositide 3-kinase/AKT pathway by utilizing focal adhesion kinase and H-Ras. Mol Cell Biol 2002;22:7015–7023.
19. Kong T, Xu D, Yu W, *et al.* G alpha 12 inhibits alpha2 beta1 integrin-mediated Madin-Darby canine kidney cell attachment and migration on collagen-I and blocks tubulogenesis. Mol Biol Cell 2009;20: 4596–4610.
20. Vogel A, Venugopalan V. Mechanisms of pulsed laser ablation of biological tissues. Chem Rev 2003;103:577–644.
21. Liu B, Li Z. Endoplasmic reticulum HSP90b1 (gp96, grp94) optimizes B-cell function via chaperoning integrin and TLR but not immunoglobulin. Blood 2008;112:1223–1230.
22. Morales C, Wu S, Yang Y, *et al.* Drosophila glycoprotein 93 is an ortholog of mammalian heat shock protein gp96 (grp94, HSP90b1, HSPC4) and retains disulfide bond-independent chaperone function for TLRs and integrins. J Immunol 2009;183:5121–5128.
23. Gonzales M, Weksler B, Tsuruta D, *et al.* Structure and function of a vimentin-associated matrix adhesion in endothelial cells. Mol Biol Cell 2001;12:85–100.
24. Ivaska J, Pallari HM, Nevo J, *et al.* Novel functions of vimentin in cell adhesion, migration, and signaling. Exp Cell Res 2007;313: 2050–2062.
25. Hirose T, Kawabuchi M, Tamaru T, *et al.* Identification of tudor repeat associator with PCTAIRE 2 (Trap). A novel protein that interacts with the N-terminal domain of PCTAIRE 2 in rat brain. Eur J Biochem 2000;267:2113–2121.
26. Conte N, Delaval B, Ginestier C, *et al.* TACC1-chTOG-Aurora A protein complex in breast cancer. Oncogene 2003;22:8102–8116.

JSHC
Japan Society of Histochemistry and Cytochemistry
Established 1959

Acta Histochem. Cytochem. 45 (1): 47–56, 2012
doi:10.1267/ahc.11057

Compensatory Upregulation of Myelin Protein Zero-Like 2 Expression in Spermatogenic Cells in Cell Adhesion Molecule-1-Deficient Mice

Hiroki Nakata[1], Tomohiko Wakayama[1], Kannika Adthapanyawanich[1], Takumi Nishiuchi[2], Yoshinori Murakami[3], Yoshimi Takai[4] and Shoichi Iseki[1]

[1]Department of Histology and Embryology, Graduate School of Medical Science, Kanazawa University, 13–1 Takara-machi, Kanazawa, Ishikawa 920–8640, Japan, [2]Division of Functional Genomics, Advanced Science Research Center, Kanazawa University, 13–1 Takaramachi, Kanazawa, Ishikawa 920–8640, Japan, [3]Division of Molecular Pathology, Department of Cancer Biology, Institute of Medical Science, The University of Tokyo, 4–6–1, Shirokanedai, Minato-ku, Tokyo 108–8639, Japan and [4]The Division of Molecular and Cellular Biology, Department of Biochemistry and Molecular Biology, Kobe University Graduate School of Medicine, Kobe, Hyogo 650–0017, Japan

Received November 14, 2011; accepted December 1, 2011; published online January 24, 2012

The cell adhesion molecule-1 (Cadm1) is a member of the immunoglobulin superfamily. In the mouse testis, Cadm1 is expressed in the earlier spermatogenic cells up to early pachytene spermatocytes and also in elongated spermatids, but not in Sertoli cells. Cadm1-deficient mice have male infertility due to defective spermatogenesis, in which detachment of spermatids is prominent while spermatocytes appear intact. To elucidate the molecular mechanisms of the impaired spermatogenesis caused by Cadm1 deficiency, we performed DNA microarray analysis of global gene expression in the testis compared between Cadm1-deficient and wild-type mice. Out of the 25 genes upregulated in Cadm1-deficient mice, we took a special interest in myelin protein zero-like 2 (Mpzl2), another cell adhesion molecule of the immunoglobulin superfamily. The levels of Mpzl2 mRNA increased by 20-fold and those of Mpzl2 protein increased by 2-fold in the testis of Cadm1-deficient mice, as analyzed with quantitative PCR and western blotting, respectively. *In situ* hybridization and immunohistochemistry demonstrated that Mpzl2 mRNA and protein are localized in the earlier spermatogenic cells but not in elongated spermatids or Sertoli cells, in both wild-type and Cadm1-deficient mice. These results suggested that Mpzl2 can compensate for the deficiency of Cadm1 in the earlier spermatogenic cells.

Key words: cell adhesion molecule, immunoglobulin superfamily, knockout mouse, spermatogenesis, testis

I. Introduction

Spermatogenesis is a complex process consisting of mitosis of spermatogonia, meiosis of spermatocytes, and transformation of spermatids (spermiogenesis) which occurs within the seminiferous tubule. It is well established that spermatogenesis is regulated by a variety of endocrine and local secretory factors [13]. Another essential factor for the regulation of spermatogenesis is cell adhesion molecules responsible for the direct interaction between spermatogenic and Sertoli cells. Apical ectoplasmic specialization (ES) is a structure formed between elongated spermatids and Sertoli cells near the apical surface of seminiferous epithelium. Several cell adhesion molecules are known to be involved in the apical ES [15, 16, 27]. Most of these molecules belong to the immunoglobulin superfamily (IGSF), which is characterized by extracellular regions that contain immunoglobulin (Ig)-like domains [2]. Studies using knockout mice have indicated that deficiency of some of

Correspondence to: Shoichi Iseki, Department of Histology and Embryology, Graduate School of Medical Science, 13–1 Takara-machi, Kanazawa 920–8640, Japan.
E-mail: siseki@med.kanazawa-u.ac.jp

the IGSF molecules, such as junctional adhesion molecule-C (Jam-C), Nectin-2 and Nectin-3, leads to male infertility due to impaired spermatogenesis [6, 8, 14].

Cell adhesion molecule-1 (Cadm1), originally reported as spermatogenic immunoglobulin superfamily (SgIGSF) [22], tumor suppressor in lung cancer 1 (Tslc1) [10] and nectin-like molecule-2 (Necl-2) [18], is a member of the IGSF and expressed in many mouse organs including the nervous system, testis, liver, and lung [24]. In the testis, Cadm1 is expressed exclusively in spermatogenic cells but not in Sertoli cells. In spermatogenic cells, Cadm1 is expressed in intermediate spermatogonia through to early pachytene spermatocytes as well as in step 7 and later spermatids, whereas it is not expressed in middle pachytene through to step 6 spermatids [23, 24, 26]. Cadm1 not only forms homophilic binding with the same molecule present on spermatogenic cells, but also heterophilic binding with another cell adhesion molecule poliovirus receptor (Pvr), that is present on Sertoli cells [23, 26]. Mice deficient for Cadm1 are infertile due to impaired spermatogenesis with markedly reduced number of mature spermatozoa [5, 20, 21, 28], indicating that the cell-cell interaction involving Cadm1 plays an indispensable role in spermatogenesis. Histologically, the seminiferous epithelium of Cadm1-deficient mice indicates prominent shedding of spermatids, particularly of step 7 to step 9 spermatids, into the lumen of seminiferous tubules [5, 21, 27, 28]. Also, the elongated spermatids remaining in the seminiferous tubules are irregular in shape and have incompletely condensed nuclei and poorly-developed flagella, indicating abnormal spermatid differentiation. In contrast, the earlier spermatogenic cells from intermediate spermatogonia through to early pachytene spermatocytes, despite the fact that these cells express Cadm1 in wild-type mice, appear to be intact. Such a phenotype of Cadm1-deficient mice may not be explained simply by the loss of cell-cell contact due to Cadm1 deficiency.

In the present study, we aimed to elucidate the molecular mechanisms underlying the impaired spermatogenesis in Cadm1-deficient mice. For this purpose, we investigated the global gene expression in the testis from Cadm1-deficient mice compared with that from wild-type mice, using the DNA microarray technique. We identified upregulation of the gene for myelin protein zero-like 2 (Mpzl2), another IGSF cell adhesion molecule, in the testis of Cadm1-deficient mice, and analyzed the expression and localization of Mpzl2 in the seminiferous tubules.

II. Materials and Methods

Animals and tissue preparation

All animal experiments were performed according to Guidelines for the Care and Use of Laboratory Animals in Kanazawa University. Cadm1-deficient 129Sv/C57BL6 strain mice (Cadm1−/−), which lack the entire exon 1 of the Cadm1 gene located on #9 autonomic chromosome, were generated as described previously [26]. Male Cadm1-deficient mice were obtained by mating the female Cadm1+/− with the male Cadm1+/−, and male wild-type mice (Cadm1+/+) were also reared for use as control. Nectin-3-deficient 129Sv/C57BL6 strain mice were generated as described previously [8]. In total, 22 Cadm1-deficient, 22 wild-type, and 3 Nectin-3-deficient male mice were used to obtain the present data. Unless otherwise indicated, the adult mice were used at the ages of 15 to 20 wk. Two female WKY/NCrj Wistar rats at 10 wk were purchased from Charles River Laboratories Japan, Inc. (Yokohama, Japan) for immunization. All animals were raised under standard laboratory conditions with a 12 hr-light/12 hr-dark cycle and free access to food and water. The mice were anesthetized with an intraperitoneal injection of sodium pentobarbital (50 mg/kg) and sacrificed by bleeding from the right atrium followed by transcardial perfusion with cold physiological saline. To isolate total RNA for microarray and reverse transcription-polymerase chain reaction (RT-PCR) or to make cell lysates for Western blotting, the testes were dissected out, frozen immediately in liquid nitrogen, and stored at −80°C until use. To make tissue sections, the animals were fixed by perfusion with cold 4% paraformaldehyde in 0.1 M phosphate buffer (pH 7.2), testes were dissected out and further fixed by immersion in the same fixative overnight at 4°C. For *in situ* hybridization (ISH) and immunohistochemistry (IHC), the fixed specimens were rinsed overnight at 4°C with 30% sucrose in 0.1 M phosphate buffer and then frozen and cut into 8 μm sections using a cryostat. Some fixed specimens were embedded in paraffin and cut into 4 μm sections for PAS-hematoxylin staining. The sections were mounted on silanized glass slides (DAKO, Glostrup, Denmark).

RNA preparation and microarray analysis

Total RNA was isolated from the testis using an acid guanidinium-based solution (TRI reagent; Sigma-Aldrich, St. Louis, MO). For the microarray analysis, total RNA of testes from 3 animals in each experimental condition were mixed to represent each total RNA sample. Microarray experiment was performed using Whole Mouse Genome oligo DNA microarray kit (Agilent Technologies, Santa Clara, CA, USA) containing 44,000 probes for mouse genes according to the manufacturer's protocol. One μg-aliquots of total RNA samples from the testes of wild-type and Cadm1-deficient mice were used to prepare Cy3- and Cy5-labeled cRNAs, respectively, using a fluorescent labeling kit (Agilent Technologies). The two sets of fluorescent labeled cRNAs were combined and purified using an RNeasy RNA purification kit (Qiagen, Hilden, Germany). After hybridization with the cRNA solution and washing, the arrays were scanned under the maximum laser intensity for both the Cy3 and Cy5 channels using an Agilent microarray scanner (G2565BA). Images were analyzed using Feature Extraction software (version 7.0; Agilent Technologies).

RT-PCR and quantitative RT-PCR

First-strand cDNA was synthesized from a 1 μg-aliquot

of the total RNA from each animal using the oligo-dT primer and reverse transcriptase (RT) (RevertraAce; Toyobo, Osaka, Japan). Using these cDNA samples, the conventional RT-PCR was performed for 28 cycles in a DNA thermal cycler (96-Well GeneAmp PCR System 9700; Applied Biosystems, Foster City, CA, USA), using Taq DNA polymerase (TaKaRa Ex Taq; Takara Bio Inc., Otsu, Shiga) and the following primer pairs: the Mpzl2 5'-primer (5'-CT ATGCAGTGTTGGCCTGAA-3'), the Mpzl2 3'-primer (5'-TGTTGAGCTGGGGGTAAAAG-3'), the glyceraldehyde-3-phosphate dehydrogenase (GAPDH) 5'-primer (5'-ACCA CAGTCCATGCCATCAC-3'), and the GAPDH 3'-primer (5'-TCCACCACCCTGTTGCTGTA-3'). The amplified products from 3 different animals were analyzed with agarose-gel electrophoresis.

Quantitative RT-PCR was performed in a Stratagene Mx-3005P thermocycler (Stratagene, La Jolla, CA, USA) according to minimum information for publication of quantitative real-time PCR experiments (MIQE). SYBR green was used to detect the amplification of cDNA in a total volume of 20 μl with the absolute quantitative, ΔCt method [17]. Each reaction consisted of 10 μl of SYBR green, 1 μl of cDNA sample, 0.5 μl of each primer pair (10 pmol/μl), and 8 μl of distilled water. Thermal cycling conditions were 10 min at 95°C followed by 45 cycles at 95°C for 40 sec, 60°C for 30 sec, and 72°C for 30 sec. GAPDH was employed as an endogenous control to normalize the data. Each sample was analyzed in triplicates, and samples from 3 different animals were analyzed to determine each value.

In situ hybridization (ISH)

An oligonucleotide containing digoxigenin (DIG)-labeled locked nucleic acid (LNA) (5'-AggGggggggaGg gagagaAataaA-3'; large capitals represent LNA) was purchased from Nippon EGT (Toyama) and used as the antisense probe for Mpzl2 mRNA. Melting temperature (Tm) of this LNA probe was predicted to be 75°C using the LNA Tm prediction tool which is accessible at http://lna-tm.com. The antisense and sense LNA probes without DIG label were also used. ISH was performed as previously described [22]. Briefly, the 4% paraformaldehyde-fixed cryostat sections of the mouse testis were treated successively at room temperature with proteinase K (10 μg/ml) in Tris-EDTA buffer for 2 min, and with 0.25% acetate anhydrate in 0.1 M triethanolamine (pH 8.0) for 10 min, washed in 4×sodium chloride/sodium citrate (SSC) and dehydrated in ethanol. The sections were then incubated with the DIG-labeled antisense probe (10 pmol/L) at 37°C for 15 hr using a hybridization buffer containing 50% deionized formamide, 2×SSC, 10 mM Tris-HCl (pH 7.5), 1 mM EDTA (pH 8.0), 1×Denhardt's solution, 0.25% SDS, 250 μg/ml yeast tRNA and 10% dextran sulfate. As control, the excess of unlabelled antisense or sense probe (1000 pmol/L) were added to DIG-labeled antisense probe. After hybridization, the tissue sections were washed in 0.2×SSC containing 2% bovine serum albumin at 37°C for 5 min. The hybridization signals were detected by incubating the sections successively with alkaline phosphatase-conjugated anti-DIG antibody (Roche Diagnostics, Basel, Switzerland) diluted at 1:600 in 0.1 M Tris-HCl, 150 mM NaCl, pH 7.5 and with the substrate Fast Red (DAKO, Glostrup, Denmark) in 50 mM Tris-HCl (pH 9.5). The ISH results were confirmed in the testes from 3 different animals. To identify the stages of seminiferous tubules, some sections were stained in the acrosome with Alexa Fluor 488-conjugated lectin PNA (1:500; Molecular Probes, Eugene, OR, USA) and counter-stained in the nucleus with bisbenzimide (Hoechst 33258; Sigma-Aldrich) at 100 ng/ml.

Preparation of primary antibodies

Rabbit polyclonal anti-Cadm1 antibody was prepared as previously described [23]. Mouse monoclonal anti-α-tubulin (clone DM 1A) antibody was purchased from Sigma-Aldrich. Rat polyclonal antisera against mouse Mpzl2 was produced in our laboratory according to the method described previously, with modification [25]. Briefly, a cDNA fragment 96 bp in length coding the carboxyl-termini of mouse Mpzl2 was cloned into the bacterial expression vector pGEX-6p-1 (Amersham Pharmacia Biotech, Uppsala, Sweden). By introducing this vector into the bacteria BL21 (Novagen, Madison, WI, USA), the recombinant oligo-peptide for Mpzl2, which was 32-amino acids in length and fused with the carrier protein glutathione-S-transferase (GST), was produced. It was then emulsified with Freund's complete adjuvant and injected as antigen into the footpads of 2 female WKY/NCrj Wistar rats. A booster immunization was made two weeks later, and sera were collected one week after the booster.

Western-blot analysis

Western blotting was performed as previously described [27]. Twenty-μg aliquots of cell lysate from the mouse testis were subjected to SDS-PAGE and transferred to PVDF membranes (Bio-Rad Laboratories, Hercules, CA, USA). The blots were incubated with rat polyclonal antisera against mouse Mpzl2 (1:2000) or mouse monoclonal anti-α-tubulin antibody (1:2000). After being washed, the blots were further incubated with horseradish peroxidase-labeled secondary antibody against rat or mouse IgG (DAKO) at 1:5000 dilution. The immunoreaction was detected and its intensity was quantified in ImageQuant LAS-4000 mini (Fujifilm Medical, Tokyo) after treatment of the blots with the chemiluminescent reagent ECL-plus (Amersham Pharmacia Biotech). Samples from 3 different animals were analyzed to determine each value.

Immunohistochemistry (IHC)

IHC at the light microscopic level was performed as previously described [26]. Briefly, the 4% paraformaldehyde-fixed cryostat sections of the mouse testis were first treated with 5% normal goat serum to prevent non-specific antibody binding and then incubated overnight at 4°C with rat polyclonal antisera against mouse Mpzl2 (1:800) for

single immunofluorescent microscopy, or with the mixture of the former antisera and rabbit polyclonal anti-Cadm1 antibody (10 μg/ml) for double immunofluorescent microscopy. For negative control, normal rat sera (1:800) were used in place of the primary antibodies. After the sections were washed in PBS, the immunoreaction was visualized by incubating the sections with anti-rat IgG antibody conjugated with Alexa Fluor 594 (Molecular Probes) at 1:400 for single immunofluorescent microscopy, or with the mixture of the former antibody and anti-rabbit IgG antibody conjugated with Alexa Fluor 488 at 1:400 for double immunofluorescent microscopy, for 1 hr at room temperature. The sections were then subjected to observation with an immunofluorescence microscope (BX50/BX-FLA; Olympus, Tokyo). The IHC results were confirmed in the testes from 3 different animals. To reveal the histological features of seminiferous tubules, the paraffin sections were stained with PAS-hematoxylin and subjected to observation with a conventional microscope.

Statistical analysis

The statistical difference between two out of multiple mean values was examined by one-factor analysis of variance (ANOVA) followed by Bonferroni's post hoc test. Differences with a P value less than 0.05 were considered significant.

III. Results

Increased expression of Mpzl2 mRNA in the testis of Cadm1-deficient mice

To elucidate the molecular mechanisms underlying the impaired spermatogenesis caused by Cadm1 deficiency, we performed DNA microarray analysis of the levels of global gene expression in the testes from Cadm1-deficient mice at 2, 5 and 20 wk postpartum compared with those from wild-type counterparts. The rationale for adopting these ages was that, during the normal testis development, pachytene spermatocytes with round shape and large nuclei first appear at 2 wk postpartum, and elongated spermatids (step 7 and later spermatids) at 5 wk postpartum, in the luminal portions of seminiferous epithelia [1]. The expressions of 25 and 21 genes were found to be increased and decreased more than 1.5-fold, respectively, at all three ages of Cadm1-deficient mice (Fig. 1A, B; Table 1). As expected, Cadm1 itself was included in the 21 down-regulated genes.

Taking into account that the testis of Cadm1-deficient mice is lacking in normal later spermatids, we considered the upregulated genes to be more worthwhile to investigate than the downregulated ones. Therefore, quantitative RT-PCR analysis was performed in the testes from adult wild-type and Cadm1-deficient mice on the mRNA for the 25 genes shown to be upregulated by DNA microarray analysis. The testis of Nectin-3-deficient mice, which are infertile due to impaired spermatogenesis, was also analyzed. We confirmed approximately 20-fold increase of the mRNA for Mpzl2 in the testis from adult Cadm1-deficient mice compared with wild-type mice (Fig. 2A, B). No significant difference was noted in the levels of Mpzl2 mRNA between wild-type and Nectin-3-deficient mice. The mRNA for Kcnd2, a potassium channel gene, was also confirmed to be increased by RT-PCR, but the mRNA for all other genes were expressed at too small copy numbers in the testis (data not shown).

Localization of Mpzl2 mRNA in the testes of wild-type and Cadm1-deficient mice

We then examined the expression and cellular localization of Mpzl2 mRNA in the testes from wild-type and Cadm1-deficient adult mice with ISH analysis. We used a digoxigenin-labeled oligonucleotide probe containing LNA, a modified DNA nucleotide. LNA probes are known to increase the melting temperature and therefore the intensity and specificity of molecular hybridization. In the seminiferous tubules of wild-type mice, the signal for Mpzl2 mRNA was detected primarily in spermatocytes but not in sperma-

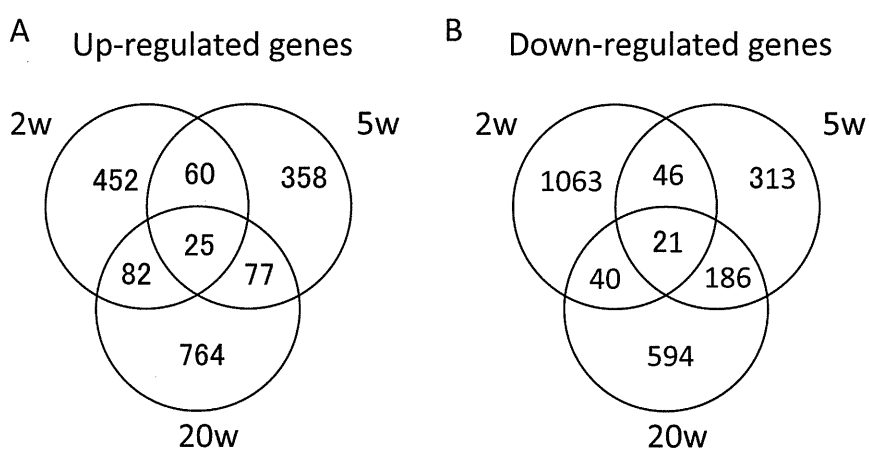

Fig. 1. Microarray analysis of the global gene expression in the testes of Cadm1-deficient mice at 2, 5 and 20 postnatal weeks (w) compared with those of wild-type mice.

Table 1. *List of up- and down-regulated genes in the testis common to all three ages of Cadm1-deficient mice compared with those of wild-type mice*

Gene	NCBI accession no.	fold change
Kcnd2	NM_019697	4.59
Mpzl2	NM_007962	4.55
		2.13
Gpr182	NM_007412	2.02
Blvrb	NM_144923	1.97
Tnfaip6	NM_009398	1.88
Trim56	NM_201373	1.85
Ei24	NM_007915	1.84
Mdk	NM_010784	1.82
Hspa8	NM_031165	1.76
Rnd2	NM_009708	1.76
Col18a1	NM_009929	1.75
Stt3a	NM_008408	1.63
Trfr2	NM_015799	1.63
Atp1a2	NM_178405	1.62
Scrn2	NM_146027	1.61
Smoc2	NM_022315	1.60
Arhgef1	NM_008488	1.57
Tnfrsf12a	NM_013749	1.56
Pla2g15	NM_133792	1.56
	AK010169	1.55
Tuba3a	NM_009446	1.55
Myoz2	NM_021503	1.52
5730437N04Rik	NM_027457	1.51
	AK085343	1.50
Prkar2a	NM_008924	0.65
	AK087842	0.65
	AK006816	0.63
	AK077682	0.63
Clec4g	NM_029465	0.62
	AK045399	0.62
Odf2	NM_013615	0.60
Rplp1	NM_018853	0.57
Ptgds	NM_008963	0.56
	BE990773	0.50
Tctex2	U21674	0.46
Fez1	NM_183171	0.44
9030425E11Rik	NM_133733	0.40
Myom2	NM_008664	0.36
Pcsk7	NM_008794	0.35
	AK007186	0.34
Hrasls5	NM_025731	0.23
Hddc3	NM_026812	0.16
Cadm1	NM_207675	0.06
Cadm1	NM_207676	0.04
Nicn1 gene	AJ299741	0.03

tids at all stages of the spermatogenesis defined by PNA lectin histochemistry (Fig. 3A, B). The signal intensity appeared to be increased in the seminiferous tubules of Cadm1-deficient mice compared with those of wild-type mice (Fig. 3C). No signal was detected in Sertoli cells, judging from the absence of signal in the basal- and apical-most portions of seminiferous epithelium. The signal disappeared when excess unlabeled antisense or sense probe was added to the probe solution for negative control (Fig. 3D).

Expression and localization of Mpzl2 protein in the testes of wild-type and Cadm1-deficient mice

Using rat polyclonal antisera against mouse Mpzl2 polypeptide, we performed western-blot analysis of cell lysates obtained from the testes of adult wild-type and Cadm1-deficient mice (Fig. 4A, B). The immunoreactive band of 70 kDa representing Mpzl2 protein was detected in the testes of both wild-type and Cadm1-deficient mice. The intensity of this signal was about 2-fold higher in Cadm1-deficient mice than in wild-type mice.

The histological features of the seminiferous tubules of Cadm1-deficient mice were first compared with those of wild-type mice in PAS-hematoxylin stained paraffin sections (Fig. 5A, B). In Cadm1-deficient mice, shedding of spermatids, particularly those later than step 7, into the seminiferous tubular lumen was prominent. The number of elongated spermatids (step 10 and later) was reduced substantially, and the remaining elongated spermatids were irregular in shape. In contrast, the earlier spermatogenic cells up to pachytene spermatocytes appeared intact.

To examine the cellular localization of Mpzl2 protein, we performed IHC in cryostat sections of the adult Cadm1-deficient and wild-type mouse testes (Fig. 6). In Cadm1-deficient mice, immunostaining for Mpzl2 was found in both the seminiferous tubules and interstitial tissue (Fig. 6A). However, the immunoreactivity in the interstitial tissue, presumably in Leydig cells, was non-specific, because replacement of the primary antibody with normal rat serum resulted in the same immunostaining (Fig. 6B). In the seminiferous tubules of Cadm1-deficient mice, the signal for Mpzl2 protein was localized to leptotene/zygotene through to early pachytene spermatocytes but was not detected in late pachytene spermatocytes through to elongated spermatids (Fig. 6C). In wild-type mice, the immunoreactive cell populations were the same as in Cadm1-deficient mice but the intensity of immunoreactivity was weaker (Fig. 6D). Double-immunofluorescence microscopy for Mpzl2 and Cadm1 in the seminiferous tubules of adult wild-type mice demonstrated that early spermatocytes express both Mpzl2 and Cadm1, whereas elongated spermatids express Cadm1 but not Mpzl2 (Fig. 7A, B, C).

IV. Discussion

Mpzl2, originally identified in mouse thymus as epithelial V-like antigen1 (EVA1), is a membrane protein with 215 amino acid residues, consisting of a signal peptide, an extracellular domain with only one Ig-like loop, a transmembrane domain, and a short intracellular domain [7]. Mpzl2 belongs to the IGS and considered to perform homophilic interaction with the same molecule. In the adult

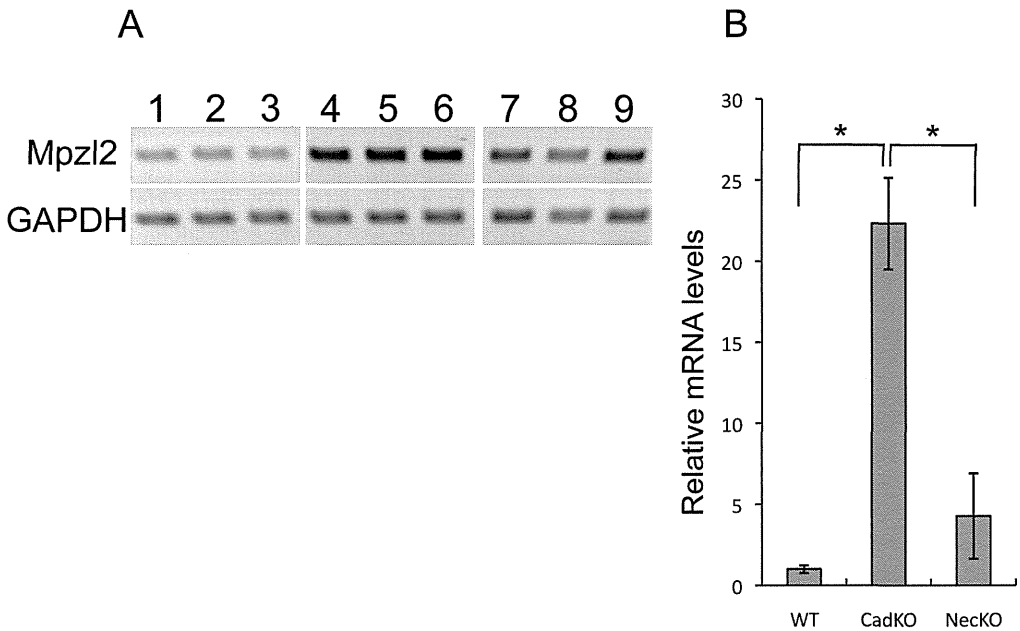

Fig. 2. (**A**) Conventional RT-PCR analysis showing the expression of Mpzl2 in the testes of wild-type (lanes1, 2, 3), Cadm1-deficient (4, 5, 6) and Nectin-3-deficient (7, 8, 9) adult mice. Amplified products from the total RNA of the testis were electrophoresed and stained with ethidium bromide. Expression of GAPDH is shown as positive control. (**B**) Realtime quantitative RT-PCR analysis showing the expression of Mpzl2 in the testes of wild-type (WT), Cadm1-deficient (CadKO) and Nectin-3-deficient (NecKO) adult mice. The relative levels of Mpzl2 mRNA adjusted with the corresponding levels of GAPDH mRNA are indicated. Each value represents mean±SD of 3 samples. *Significantly different (P<0.01).

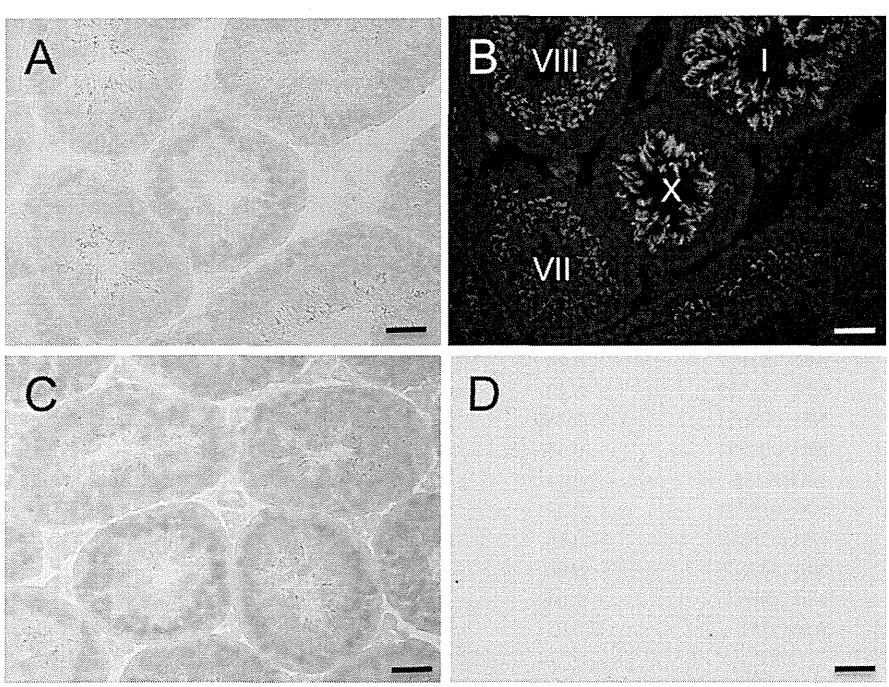

Fig. 3. (**A, C, D**) ISH analysis of the expression and localization of Mpzl2 mRNA in the testes of wild-type (**A, D**) and Cadm1-deficient (**C**) adult mice. Cryostat sections were hybridized with Dig-labeled antisense Mpzl2 probe in the absence (**A, C**) and presence (**D**) of excess unlabeled antisense probe, and the hybridization signal was visualized with alkaline-phosphatase histochemistry. (**B**) The same section as (**A**) was stained in the acrosomes with the PNA lectin histochemistry and in the nuclei with bisbenzimide. The spermatogenic stages of the seminiferous tubules are shown with roman numerals. Bar=50 μm.

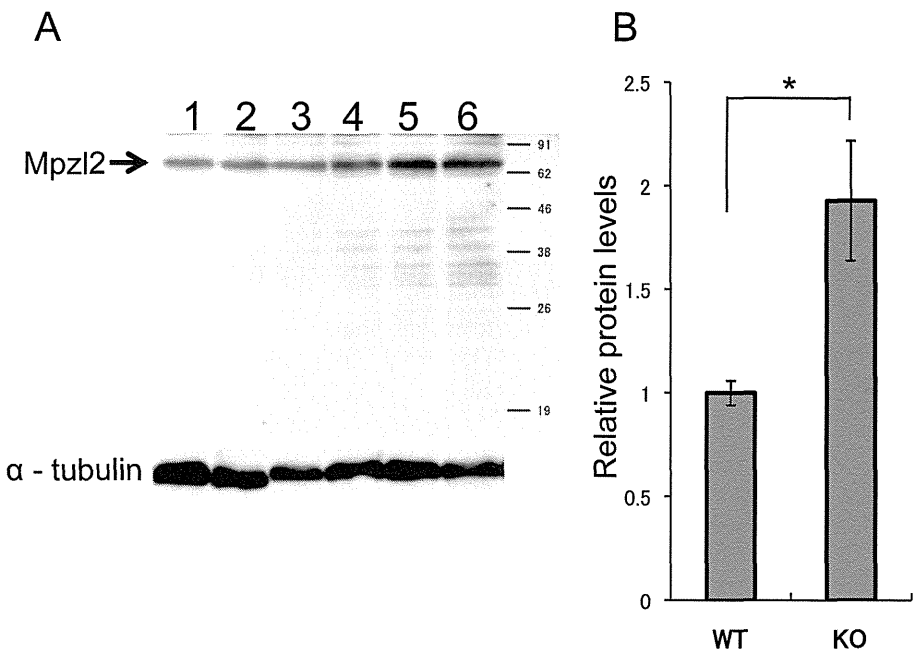

Fig. 4. Western blot analysis of the expression of Mpzl2 protein in the testes of wild-type (lanes 1, 2, 3) and Cadm1-deficient (4, 5, 6) adult mice. (**A**) The protein samples were electrophoresed, blotted and immunostained with rat anti-Mpzl2 antisera. For the control, staining with mouse anti-α-tubulin antibody was also performed. The molecular weight scale is shown. (**B**) The relative levels of Mpzl2 in the wild-type (WT) and Cadm1-deficient (KO) mice adjusted with the corresponding levels of α-tubulin. Each value represents mean±SD of 3 samples. *Significantly different ($P<0.01$).

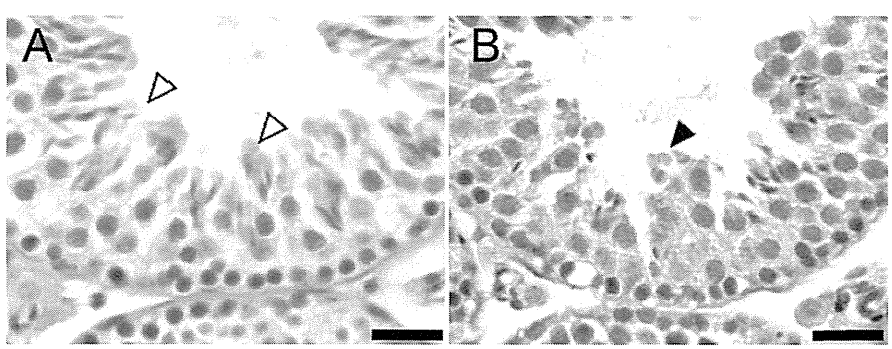

Fig. 5. Histological features of the seminiferous tubules of wild-type (**A**) and Cadm1-deficient (**B**) adult mice. Paraffin sections of the testes were stained with the PAS-hematoxylin method. Note that the elongated spermatids are lower in number and irregular in shape (black arrowhead) in Cadm1-deficient mouse, as compared with the normal step 12 elongated spermatids (white arrowheads) in wild-type mouse. Bar=50 μm.

mouse organs, Mpzl2 is expressed in the gut, kidney, liver, skin, testis, and thymus [7]. In the thymus, Mpzl2 is considered to be involved in the lymphocyte-stromal cell interaction, because it is expressed in thymocytes in the embryonic ages but in epithelial cells in the postnatal ages [4]. Transgenic mice overexpressing Mpzl2 in cortical epithelial cells of the thymus show increases in the size and absolute cell number of thymus, in spite of an increase of apoptosis in the thymus. Also, Mpzl2 is expressed in epithelial cells of the human choroid plexus and may play a role in the regulation of permeability in the choroid plexus barrier [3]. So far, no report is available on the generation of the knock-out mouse for Mpzl2, thus it is unknown if Mpzl2 is indispensable for spermatogenesis.

In the present results, the levels of Mpzl2 mRNA increased by 20-fold and those of Mpzl2 protein increased by 2-fold in the testis from Cadm1-deficient mice compared with that from wild-type mice. Other cell adhesion molecules known to be expressed in spermatogenic cells, such as N-cadherin (N-cad), Coxsackievirus and adenovirus receptor (CAR), Jam-C, and Nectin-3 [27], were not detected among the 25-up-regulated genes in microarray. We also confirmed

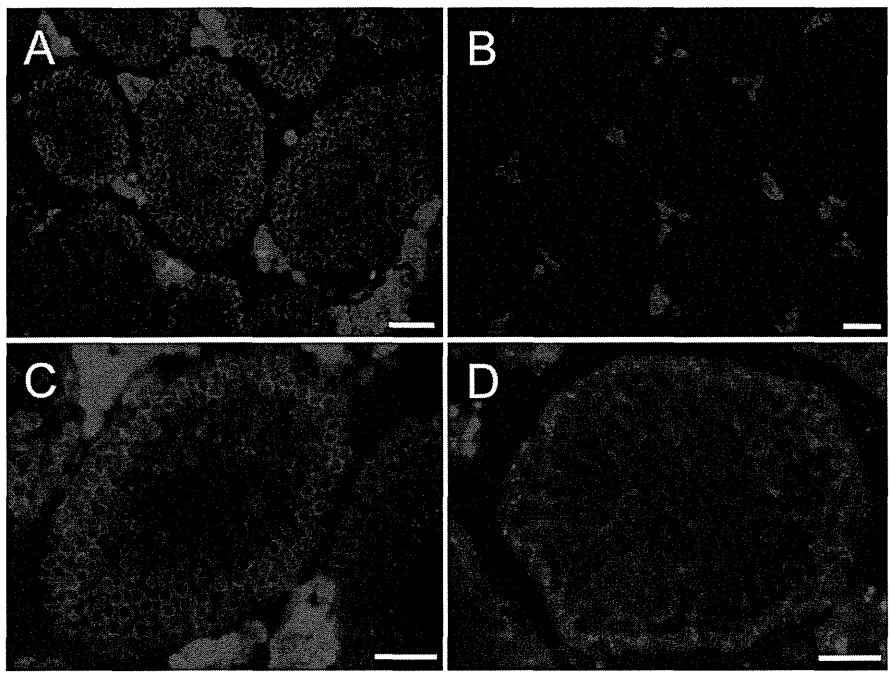

Fig. 6. Immunohistochemical localization of Mpzl2 in the testes of Cadm1-deficient (**A, B, C**) and wild-type (**D**) adult mice. Cryostat sections were immunostained with rat anti-Mpzl2 antisera (**A, C, D**) or non-immune rat serum (**B**). Note that the reactivity in the interstitial cells are detected without the primary antibody and thus is nonspecific. In both mice, Mpzl2-immunoreactivity is primarily localized in the earlier spermatogenic cells up to early pachytene spermatocytes. Bar=50 μm.

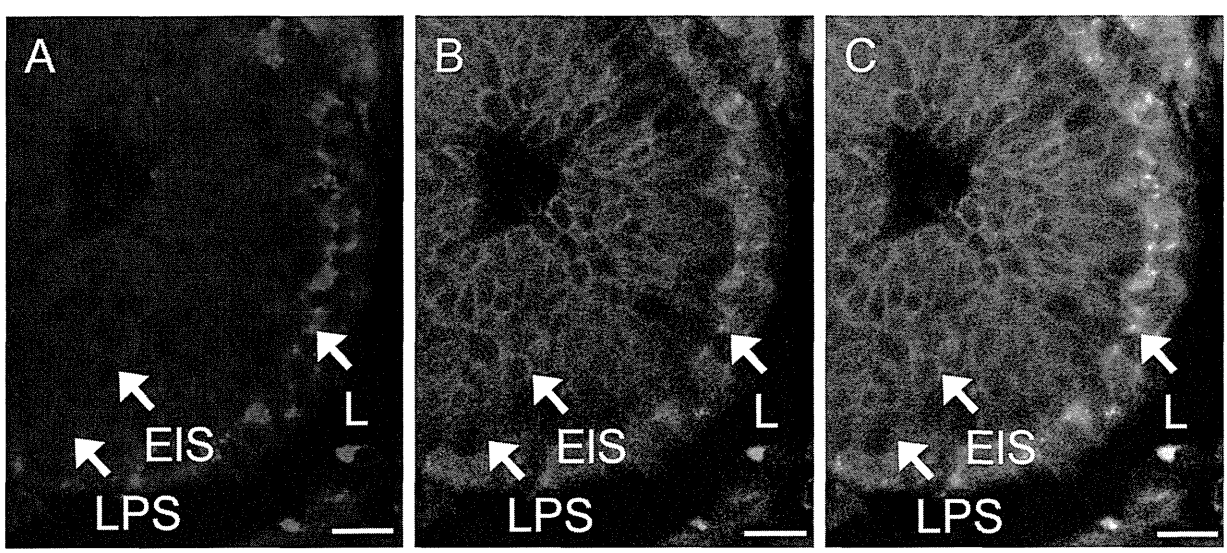

Fig. 7. Double immunostaining of the stage IX seminiferous tubule of a wild-type adult mouse with rat polyclonal anti-Mplz2 antisera and rabbit polyclonal anti-Cadm1 antibody. Note that in leptotene spermatocytes (L) the immunoreactivity for Mpzl2 (red, **A**) overlaps with that of Cadm1 antibody (green, **B**) when merged (yellow, **C**). In contrast, elongated spermatids (ElS) are immunopositive for Cadm1 but negative for Mpzl2, and late pachytene spermatocytes (LPS) are negative for both Mpzl2 and Cadm1. Bar=20 μm.

with RT-PCR that none of the mRNA for these adhesion molecules were increased in the testis from Cadm1-deficient mice (data not shown). Furthermore, Mpzl2 mRNA showed no increase in the testis from Nectin-3-deficient mice, which also has impaired spermatogenesis. Taken together, these results suggest that the upregulation of Mpzl2 expression in Cadm1-deficient mouse testis is a specific phenomenon. The precise mechanisms underlying this upregulation are unclear. Although both of the genes for Mpzl2 and Cadm1 are located on chromosome 9, their distance is as long as

2.5×10^6 nucleotides, their promoter regions are different, and their transcriptional control in the testis is largely unknown.

ISH demonstrated that the Mpzl2 mRNA is primarily expressed in the spermatocytes, and IHC further demonstrated that the Mpzl2 protein is localized in the leptotene/zygotene through to early pachytene spermatocytes in both wild-type and Cadm-1-deficient mice. It should be noted that Cadm1-deficient mice have impaired spermatogenesis accompanied by prominent shedding of elongated spermatids into the lumen of seminiferous tubules, whereas the earlier spermatogenic cells up to early pachytene spermatocytes appeared intact. The presence of Mpzl2 in Cadm1-positive earlier spermatogenic cells in contrast with the absence of Mpzl2 in Cadm1-positive elongated spermatids leads us to the hypothesis that Mpzl-2 and Cadm1 have functional redundancy in the seminiferous tubules. The deficiency of Cadm1 may be compensated for by the increased amount of Mpzl2 in the earlier spermatogenic cells, whereas such compensation may not work in Mpzl2-negative elongated spermatids, resulting in their detachment from Sertoli cells.

Elongated spermatids express, besides Cadm1, all of N-cad, CAR, Jam-C, and Nectin-3. Among these cell adhesion molecules, Jam-C and Nectin-3, when deficient, cause the shedding of elongated spermatids as well as the malformation of the remaining elongated spermatids, similar to Cadm1 [6, 8]. Interestingly, Jam-C and Nectin-3, as well as Cadm1, have both homophilic and heterophilic binding activities, and interact not only with the same molecules but also with Jam-B, Nectin-2, and Pvr, respectively, that are expressed in Sertoli cells [27]. These adhesion molecules, that are expressed in elongated spermatids and indispensable for spermatogenesis, appear to be unable to compensate for the lack of the others. On the other hand, early spermatocytes have been known to express, besides Cadm1, no Jam-C or Nectin-3 but N-cad and CAR [9, 12]. N-cad and CAR are also expressed in Sertoli cells and can be involved in the interaction between spermatogenic and Sertoli cells through homophilic binding. However, considering that N-cad [11] and CAR are unable to compensate for the lack of Cadm1, Jam-C or Nectin-3 in elongated spermatids, they are more likely responsible for the interaction between Sertoli cells. Since the present ISH results indicated that Mpzl2 is not expressed in Sertoli cells, the compensatory function of Mpzl2 on Cadm1 may be based on its heterophilic binding with Pvr, the known binding partner of Cadm1, or some other yet unidentified adhesion molecule present on Sertoli cells. So far, no molecule has been reported as the heterophilic binding partner of Mpzl2. Further studies are required to clarify this issue. On the other hand, the homophilic binding activity of Mpzl2, as well as that of Cadm1, JamC and Nectin-3, might be responsible for the interaction among spermatogenic cells for their synchronized development.

Spermatogenesis [19] is a process by which spermatogenic stem cells give rise to highly differentiated spermatozoa through the interaction of spermatogenic cells with somatic Sertoli cells. This process may require many cell adhesion molecules expressed on the surface of spermatogenic and Sertoli cells. The present study suggested that there is a complex functional redundancy among these adhesion molecules. In the case of the deficiency of one of these molecules, the presence or absence of compensation of the deficient molecule with another molecule may bring about a variety of phenotypes in seminiferous tubules. The double-knockout study targeting various combinations of these molecules may shed light on the biological significance of each molecule in spermatogenesis. To date only a few cell adhesion molecules have been proven to be essential for spermatogenesis. Although human male infertility is often idiopathic, some infertile patients may have defective spermatogenesis due to dysfunction of some of these cell adhesion molecules. We hope to identify such molecules in the future.

V. Acknowledgments

This work was supported by a Grant-in-Aid from the Ministry of Education, Science, and Culture of Japan, and by the Honjin Foundation to TW.

VI. References

1. Bellvé, A. R., Cavicchia, J. C., Millette, C. F., O'Brien, D. A., Bhatnagar, Y. M. and Dym, M. (1997) Spermatogenic cells of the prepuberal mouse. Isolation and morphological characterization. *J. Cell Biol.* 74; 68–85.
2. Brümmendorf, T. and Rathjen, F. G. (1995) Cell adhesion molecules 1: immunoglobulin superfamily. *Protein Profile* 2; 963–1108.
3. Chatterjee, G., Carrithers, L. M. and Carrithers, M. D. (2008) Epithelial V-like antigen regulates permeability of the blood-CSF barrier. *Biochem. Biophys. Res. Commun.* 372; 412–417.
4. DeMonte, L., Porcellini, S., Tafi, E., Sheridan, J., Gordon, J., Depreter, M., Blair, N., Panigada, M., Sanvito, F., Merati, B., Albientz, A., Barthlott, T., Ozmen, L., Blackburn, C. C. and Guttinger, M. (2007) EVA regulates thymic stromal organisation and early thymocyte development. *Biochem. Biophys. Res. Commun.* 356; 334–340.
5. Fujita, E., Kouroku, Y., Ozeki, S., Tanabe, Y., Toyama, Y., Maekawa, M., Kojima, N., Senoo, H., Toshimori, K. and Momoi, T. (2006) Oligo-astheno-teratozoospermia in mice lacking RA175/TSLC1/SynCAM/IGSF4A, a cell adhesion molecule in the immunoglobulin superfamily. *Mol. Cell. Biol.* 26; 718–726.
6. Gliki, G., Ebnet, K., Aurrand-Lions, M., Imhof, B. A. and Adams, R. H. (2004) Spermatid differentiation requires the assembly of a cell polarity complex downstream of junctional adhesion molecule-C. *Nature* 431; 320–324.
7. Guttinger, M., Sutti, F., Panigada, M., Porcellini, S., Merati, B., Mariani, M., Teesalu, T., Consalez, G. G. and Grassi, F. (1998) Epithelial V-like antigen (EVA), a novel member of the immunoglobulin superfamily, expressed in embryonic epithelia with a potential role as homotypic adhesion molecule in thymus histogenesis. *J. Cell Biol.* 141; 1061–1071.
8. Inagaki, M., Irie, K., Ishizaki, H., Tanaka-Okamoto, M., Miyoshi, J. and Takai, Y. (2006) Role of cell adhesion molecule nectin-3 in spermatid development. *Genes Cells* 11; 1125–1132.
9. Johnson, K. J. and Boekelheide, K. (2002) Dynamic testicular

adhesion junctions are immunologically unique. II. Localization of classic cadherins in rat testis. *Biol. Reprod.* 66; 992–1000.
10. Kuramochi, M., Fukuhara, H., Nobukuni, T., Kanbe, T., Maruyama, T., Ghosh, H. P., Pletcher, M., Isomura, M., Onizuka, M., Kitamura, T., Sekiya, T., Reeves, R. H. and Murakami, Y. (2001) TSLC1 is a tumor-suppressor gene in human non-small-cell lung cancer. *Nat. Genet.* 27; 427–430.
11. Kusumoto, K., Kikuchi, M., Fujiwara, K., Horiguchi, K., Kouki, T., Kawanishi, K. and Yashiro, T. (2010) Effect of E-cadherin expression on hormone production in rat anterior pituitary lactotrophs in vitro. *Acta Histochem. Cytochem.* 43; 83–88.
12. Mirza, M., Hreinsson, J., Strand, M. L., Hovatta, O., Söder, O., Philipson, L., Pettersson, R. F. and Sollerbrant, K. (2006) Coxsackievirus and adenovirus receptor (CAR) is expressed in male germ cells and forms a complex with the differentiation factor JAM-C in mouse testis. *Exp. Cell Res.* 312; 817–830.
13. O'Donnell, L., Meachem, S. J., Stanton, P. G. and McLachlan, R. I. (2006) Endocrine regulation of spermatogenesis. In "Knobil and Neill's Physiology of Reproduction, 3rd ed", ed. by J. D. Neill, Academic Press, New York, pp. 1017–1069.
14. Ozaki-Kuroda, K., Nakanishi, H., Ohta, H., Tanaka, H., Kurihara, H., Mueller, S., Irie, K., Ikeda, W., Sakai, T., Wimmer, E., Nishimune, Y. and Takai, Y. (2002) Nectin couples cell-cell adhesion and the actin scaffold at heterotypic testicular junctions. *Curr. Biol.* 12; 1145–1150.
15. Sakisaka, T. and Takai, Y. (2004) Biology and pathology of nectins and nectin-like molecules. *Curr. Opin. Cell Biol.* 16; 513–521.
16. Salanova, M., Ricci, G., Boitani, C., Stefanini, M., De Grossi, S. and Palombi, F. (1998) Junctional contacts between Sertoli cells in normal and aspermatogenic rat seminiferous epithelium contain alpha6beta1 integrins, and their formation is controlled by follicle-stimulating hormone. *Biol. Reprod.* 58; 371–378.
17. Schmittgen, T. D. and Livak, K. J. (2008) Analyzing real-time PCR data by the comparative C(T) method. *Nat. Protoc.* 3; 1101–1108.
18. Shingai, T., Ikeda, W., Kakunaga, S., Morimoto, K., Takekuni, K., Itoh, S., Satoh, K., Takeuchi, M., Imai, T., Monden, M. and Takai, Y. (2003) Implications of nectin-like molecule-2/IGSF4/RA175/SgIGSF/TSLC1/SynCAM1 in cell-cell adhesion and transmembrane protein localization in epithelial cells. *J. Biol. Chem.* 278; 35421–35427.
19. Song, N., Liu, J., An, S., Nishino, T., Hishikawa, Y. and Koji, T. (2011) Immunohistochemical analysis of histone H3 modifications in germ cells during mouse spermatogenesis. *Acta Histochem. Cytochem.* 44; 183–190.
20. Surace, E. I., Strickland, A., Hess, R. A., Gutmann, D. H. and Naughton, C. K. (2006) Tslc1 (nectin-like molecule-2) is essential for spermatozoa motility and male fertility. *J. Androl.* 27; 816–825.
21. Van der Weyden, L., Arends, M. J., Chausiaux, O. E., Ellis, P. J., Lange, U. C., Surani, M. A., Affara, N., Murakami, Y., Adams, D. J. and Bradley, A. (2006) Loss of TSLC1 causes male infertility due to a defect at the spermatid stage of spermatogenesis. *Mol. Cell. Biol.* 26; 3595–3609.
22. Wakayama, T., Ohashi, K., Mizuno, K. and Iseki, S. (2001) Cloning and characterization of a novel mouse immunoglobulin superfamily gene expressed in early spermatogenic cells. *Mol. Reprod. Dev.* 60; 158–164.
23. Wakayama, T., Koami, H., Ariga, H., Kobayashi, D., Sai, Y., Tsuji, A., Yamamoto, M. and Iseki, S. (2003) Expression and functional characterization of the adhesion molecule spermatogenic immunoglobulin superfamily in the mouse testis. *Biol. Reprod.* 68; 1755–1763.
24. Wakayama, T., Koami, H., Yamamoto, M. and Iseki, S. (2004) Expression of the adhesion molecule spermatogenic immunoglobulin superfamily (SgIGSF). *Acta Histochem. Cytochem.* 37; 365–371.
25. Wakayama, T., Kato, Y., Usumi, R., Tsuji, A. and Iseki, S. (2006) A time and cost-saving method of producing rat polyclonal antibodies. *Acta Histochem. Cytochem.* 39; 79–87.
26. Wakayama, T., Sai, Y., Ito, A., Kato, Y., Kurobo, M., Murakami, Y., Nakashima, E., Tsuji, A., Kitamura, Y. and Iseki, S. (2007) Heterophilic binding of the adhesion molecules poliovirus receptor and immunoglobulin superfamily 4A in the interaction between mouse spermatogenic and Sertoli cells. *Biol. Reprod.* 76; 1081–1090.
27. Wakayama, T. and Iseki, S. (2009) Role of the spermatogenic-Sertoli cell interaction through cell adhesion molecule-1 (CADM1) in spermatogenesis. *Anat. Sci. Int.* 84; 112–121.
28. Yamada, D., Yoshida, M., Williams, Y. N., Fukami, T., Kikuchi, S., Masuda, M., Maruyama, T., Ohta, T., Nakae, D., Maekawa, A., Kitamura, T. and Murakami, Y. (2006) Disruption of spermatogenic cell adhesion and male infertility in mice lacking TSLC1/IGSF4, an immunoglobulin superfamily cell adhesion molecule. *Mol. Cell. Biol.* 26; 3610–3624.

Cancer Science
The official journal of the Japanese Cancer Association JCA

Expression of a splicing variant of the *CADM1* specific to small cell lung cancer

Shinji Kikuchi,[1,2,6] Miwako Iwai,[1,6] Mika Sakurai-Yageta,[1] Yumi Tsuboi,[1] Takeshi Ito,[1] Tomoko Maruyama,[1] Hitoshi Tsuda,[3] Yae Kanai,[4] Masataka Onizuka,[2] Yukio Sato[2] and Yoshinori Murakami[1,5]

[1]Division of Molecular Pathology, Institute of Medical Science, The University of Tokyo, Tokyo; [2]Department of Thoracic Surgery, Faculty of Medicine, University of Tsukuba, Tsukuba; [3]Department of Diagnostic Pathology, National Cancer Research Center Hospital, Tokyo; [4]Division of Pathology, National Cancer Research Center Research Institute, Tokyo, Japan

(Received December 29, 2011/Revised March 1, 2012/Accepted March 4, 2012/Accepted manuscript online March 20, 2012/Article first published online May 15, 2012)

CADM1, a member of the immunoglobulin superfamily cell adhesion molecule, acts as a tumor suppressor in a variety of human cancers. CADM1 is also ectopically expressed in adult T-cell leukemia (ATL), conferring an invasive phenotype characteristic to ATL. Therefore, CADM1 plays dual roles in human oncogenesis. Here, we investigate the roles of CADM1 in small cell lung cancer (SCLC). Immunohistochemistry demonstrates that 10 of 35 (29%) primary SCLC tumors express CADM1 protein. Western blotting and RT-PCR analyses reveal that CADM1 is significantly expressed in 11 of 14 SCLC cells growing in suspension cultures but in neither of 2 SCLC cells showing attached growth to plastic dishes, suggesting that CADM1 is involved in anchorage-independent growth in SCLC. In the present study, we demonstrate that SCLC expresses a unique splicing variant of CADM1 (variant 8/9) containing additional extracellular fragments corresponding to exon 9 in addition to variant 8, a common isoform in epithelia. Variant 8/9 of CADM1 is almost exclusively observed in SCLC and testis, although this variant protein localizes along the membrane and shows similar cell aggregation activity to variant 8. Interestingly, both variant 8/9 and variant 8 of CADM1 show enhanced tumorigenicity in nude mice when transfected into SBC5, a SCLC cell lacking CADM1. Inversely, suppression of CADM1 expression by shRNA reduced spheroid-like cell aggregation of NCI-H69, an SCLC cell expressing a high amount of CADM1. These findings suggest that CADM1 enhances the malignant features of SCLC, as is observed in ATL, and could provide a molecular marker specific to SCLC. (*Cancer Sci* 2012; 103: 1051–1057)

Small cell lung cancer (SCLC) is one of the cancers that is refractory to therapeutic approaches, although patients with SCLC often respond favorably to combined modality chemotherapy at the initial treatment.[1] To date, a molecular targeting therapy has not been developed for SCLC. Therefore, novel approaches to the diagnosis and treatment of SCLC on the basis of molecular alterations would be a prerequisite to control this refractory cancer. One of the most critical phenotypes to determine the prognosis of SCLC patients is its metastatic ability to distant organs, even in the very early stages of the disease. Corresponding to its metastatic phenotype, cultured cells from SCLC poorly adhere to plastic dishes and often grow in suspension. Thus, in spite of its epithelial origin, SCLC cells could also be categorized as cancer cells of less adhesive activity, such as lymphoma and leukemia.[2] It is well known that the *TP53* and the *RB1* genes are inactivated in the majority of SCLC. In addition, promoter methylation of the *RASSF1*, point mutation of the *KRAS2* and inactivation of the *MYO18B* genes are detected in a significant portion of SCLC.[3,4] It is also reported that the genetic polymorphisms in the *MTH1* gene are associated with the risk of SCLC.[5] Disrupted functions of these gene products would be involved in the malignant features of SCLC. However, molecules directly involved in anchorage-independent growth of SCLC cells, especially those involved in cell adhesion, are not well investigated in SCLC.

The *CADM1* on chromosomal fragment 11q23.2 was initially identified as a tumor suppressor in non-SCLC (NSCLC) by its tumor suppressor activity in nude mice.[6,7] *CADM1* encodes an immunoglobulin superfamily cell adhesion molecule (IgCAM) expressed in the brain, testis, lung and various epithelial tissues. The CADM1 protein plays important roles in epithelial cell adhesion through its homophilic trans-interaction between the adjacent cells.[8] In contrast, CADM1 expression is frequently lost in various cancers in their invasive lesions. In fact, *CADM1* inactivation by promoter methylation was observed in 44% of NSCLC[9] and 20–50% of human tumors from prostate,[10] breast,[11] pancreas,[12] stomach,[13] esophagus,[14] nasopharynx[15] and uterine cervix.[16] CADM1 associates with an actin-binding protein, 4.1B/DAL-1,[17] and a member of the scaffold proteins, membrane-associated guanylate kinases, including MPP1, MPP2, MPP3, CASK and Pals2.[18–20] Loss of 4.1B or MPP3 in NSCLC, renal cancer and meningioma strongly suggests that 4.1B and MPP3 are downstream targets of CADM1 when it acts as a tumor suppressor in epithelial tissues.[17,18,21–23]

In contrast, CADM1 is reported to be ectopically expressed in adult T-cell leukemia (ATL) cells, providing a possible diagnostic marker for ATL.[24] Moreover, CADM1-mediated adhesion between ATL cells and fibroblasts or endothelial cells appears to promote invasion into the skin or various organs, which are characteristic features of ATL.[25] We recently demonstrated that, in ATL cells, CADM1 associates with Tiam1, a Rac-specific guanine nucleotide exchange factor, and promotes cell invasion by interacting with fibroblasts or endothelial cells *in vitro*.[26] By associating with a distinct series of downstream molecules, CADM1 appears to play dual roles in human oncogenesis: as a tumor suppressor in epithelial cancers and as an oncoprotein that promotes invasion in ATL cells.

In the present study, we demonstrate the high incidence of CADM1 overexpression in SCLC and its strong correlation with anchorage-independent cell growth. Enhancement of tumorigenicity in nude mice by CADM1 suggests that CADM1 acts as an oncoprotein that promotes malignant growth in SCLC cells, as was reported in ATL cells. Furthermore, a splicing variant of CADM1 that we found in SCLC cells is highly specific to SCLC, except for testis. CADM1 could provide a novel molecular target for the diagnosis and growth suppression of SCLC cells.

[5]To whom correspondence should be addressed.
E-mail: ymurakam@ims.u-tokyo.ac.jp
[6]These authors contributed equally to this work.

doi: 10.1111/j.1349-7006.2012.02277.x

Materials and Methods

Tumor samples, cell lines and animals. Five primary NSCLC tumors and a primary SCLC tumor, as well as corresponding non-cancerous tissues from the same patients, were surgically resected and histologically diagnosed at the Department of Diagnostic Pathology, National Cancer Research Center Hospital, Japan. Human samples were analyzed in accordance with the institutional guidelines (IMSUT 20–36). A total of 16 SCLC and 10 NSCLC cells were obtained, as described in Supplementary Table S1. The cells were cultured according to the suppliers' recommendation. BALB/cA-nu (nu/nu) mice were from Charles River Laboratories Japan (Yokohama, Japan). All animal experiments were performed according to the Guidelines for Animal Experiments at the University of Tokyo.

RT-PCR analysis. Human adult lung and brain poly-A^+ RNA was obtained from Clontech (Palo Alto, CA, USA). Poly-A^+ RNA and total cellular RNA were extracted using the FastTrack 2.0 Kit (Invitrogen, Carlsbad, CA, USA) and reverse-transcribed by Superscript II (Invitrogen), as described previously.[9] Primers used for amplification of a 150-bp fragment of CADM1 are 5′-TTTTCTAGCAGTGAACTCAAA-GTATCAT-3′ (sense) and 5′-GATATCGATCATCAGATTAC-GTGGTG-3′ (anti-sense), while those of a 646-bp fragment of beta-actin as an internal control in the same reaction are 5′-AAATCTGGCACCACACCTT-3′ (sense) and 5′-AGCACT-GTGTTGGCGTACAG-3′ (anti-sense). For quantitative RT-PCR analysis, real-time monitoring of a PCR reaction of 55 cycles was performed using the Light Cycler system (Roche Molecular Systems, Indianapolis, IN, USA) and the Light Cycler Fast Start DNA SYBR Green I kit according to the manufacturer's instructions. Relative expression of CADM1 was measured in three independent experiments.

Analysis of splicing variants. cDNA fragments of CADM1 corresponding to exons 7-11 were amplified by PCR using a pair of primers, 5′-GTGATGGTAACTTGGGTGAGAGTC-3′ (sense) and 5′-CCAGAATGATGAGCAAGCACAG-3′ (anti-sense). The 5′ end of the sense primer was labeled with Texas Red, and PCR was carried out as described previously.[9] After denaturing at 95°C for 3 min, the PCR product was subjected to PAG containing 6 M urea for 180 min at 45°C using SF5200 (Hitachi Electronics Engineering, Tokyo, Japan), with cooling systems as described previously.[9] The results were analyzed using a DNA Fragment Analyzer (Hitachi Electronics Engineering).

Western blotting and deglycosylation. Western blotting was performed as described previously[8] using a rabbit anti-CADM1 polyclonal antibody (pAb) (CC2) and a goat anti-GAPDH pAb (V-18; Santa Cruz Biotechnology, Santa Cruz, CA, USA) as a control. N-linked glycans were digested by peptide *N*-glycosidase F (New England Biolabs, Beverly, MA, USA) as described previously.[27] Briefly, 20 μg of protein from cell lysates in a 90 μL lysis buffer was denatured with 10 μL of a glycoprotein denaturing buffer (5% SDS, 10% beta-mercaptoethanol) at 100°C for 10 min and then incubated with 10 μL of a G7 buffer (0.5 M sodium phosphate, pH 7.5) and 10 μL of 10% NP-40 containing 1500 U of peptide *N*-glycosidase F at 37°C for 5 h.

Immunohistochemistry. Paraffin sections of primary SCLC were purchased from Cybrdi (Gaithersburg, MD, USA). The sections were incubated with a rabbit anti-CADM1 pAb (CC2) and visualized by Envision kit/HRP (DAB) (Dako) as described previously.[28] All sections were counterstained with hematoxylin. For analyses of the subcellular localization of CADM1, cells were seeded on culture slides for 2–3 days, permeabilized and stained with anti-CADM1 pAb(CC2). CADM1 protein and actin filaments were visualized with Alexa Flour 488-conjugated anti-rabbit IgG and Alexa Flour 568 phalloidine, respectively, and detected by a Biozero BZ-8000 (Keyence, Tokyo, Japan).

Plasmids and transfection. Splicing variants of CADM1 containing the sequences corresponding to exons 7, 8 and 11 (variant 8) (3, 25) and exons 7, 8, 9 and 11 (variant 8/9) were cloned into the expression vector pcDNA3.1 (Invitrogen). Transfection was carried out using FuGENE 6 (Roche Diagnostics, Indianapolis, IN, USA) and stable cell clones were selected against 200 μg/mL of hygromycin.

Cell aggregation assay. A cell suspension (1×10^5 cell/well) in normal HBSS with Ca^{2+} and Mg^{2+} or HBSS without Ca^{2+} and Mg^{2+} was reseeded in Ultra Low Cluster six-well plates (Corning Incorporated, Corning, NY, USA) and rotated at 37°C for 20–60 min, as described previously.[8] The extent of aggregation of cells was represented by the ratio of the total particle number at time t of incubation (N_t) to the initial particle number (N_0).

RNAi. The siRNA sequences targeting CADM1 were from position +194 to +212 and +204 to +222 of the CADM1 mRNA relative to the first adenine of the initiation codon at position 1. For constructing an expression vector of CADM1 siRNA, ribonucleotides of the above sequence were synthesized and cloned into pSilencer 3.0-H1 (Ambion, Austin, TX, USA) to generate the shRNA, followed by the insertion of the neomycin resistance gene into the vector at the SspI site. Then, the CADM1 shRNA expression vector or pSilencer-negative control-neo siRNA (Ambion) was transfected into NCI-H69 cells using DMRIE-C (Invitrogen) and selected against 500 μg/mL of G418 in the culture medium for 14 days to obtain the pooled clones.

Analysis of tumorigenicity. A suspension of 1×10^6 cells in PBS (0.2 mL) was subcutaneously injected into the flanks of 5–6-week-old female BALB/cA-nu (nu/nu) mice. Tumor size was measured twice weekly using a Vernier caliper. Tumor volume (V) was calculated using the values of the largest (A) and smallest (B) diameters according to the formula $V = 0.5 \times AB^2$.

Statistical analysis. Experimental differences were tested for statistical significance using the independent t-test. The software Stat View 5.0 (SAS Institute, Cary, NC, USA) was used for the analysis. Differences with P-values of <0.05 were considered significant.

Results

Expression of CADM1 in small cell lung cancer. Expression of the *CADM1* in 16 SCLC and 10 NSCLC cells was examined by quantitative RT-PCR (Fig. 1a and Fig. S1). A significant amount of CADM1 mRNA was detected in 14 of 16 (88%) SCLC cells, whereas CADM1 mRNA was reduced or absent in all 10 NSCLC cells, as reported previously.[6] Interestingly, 2 SCLC cells, SBC3 and SBC5, lacking CADM1 expression, grew attached to the plastic dishes, similarly to all 10 NSCLC cells examined. In contrast, all 14 SCLC cells expressing CADM1 mRNA showed anchorage-independent growth, providing a strong association between CADM1 expression and the growth ability in suspension ($P < 0.0001$). Western blotting revealed that 11 of 14 SCLC cells showed a considerable amount of CADM1 protein. However, CADM1 protein is absent in SBC3 and SBC5, as well as in 9 NSCLC cells (Fig. 1b). Immunohistochemical studies revealed that CADM1 was highly expressed along the cell–cell attachment sites in 10 of 35 (29%) primary SCLC (Fig. S2).

Identification of the splicing variant of CADM1 in small cell lung cancer. Broad signals for CADM1 from SCLC cells in western blotting suggested possible glycosylation (Fig. 1b). Thus, 4 SCLC cells, NCI-H69, NCI-H510, Lu134 and Lu139,

doi: 10.1111/j.1349-7006.2012.02277.x

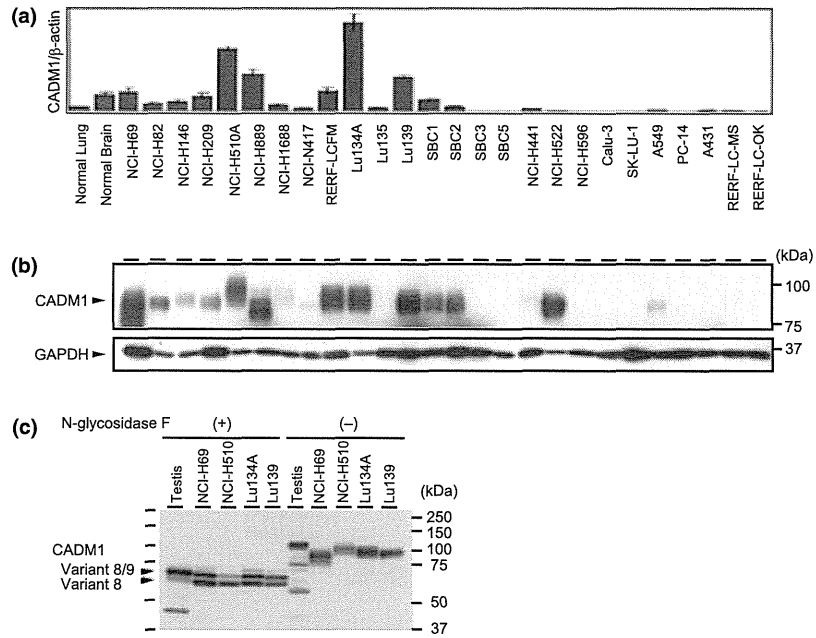

Fig. 1. Expression of CADM1 in small cell lung cancer (SCLC) and non-SCLC (NSCLC). (a) Quantitative RT-PCR analysis of CADM1 mRNA in SCLC and NSCLC cells. The intensity of CADM1 mRNA was normalized to that of β-actin. Columns represent the mean ± SD (bars). The data were obtained from three independent experiments. (b) Western blotting of CADM1 protein in SCLC and NSCLC cells. CADM1 was detected by anti-CADM1 polyclonal antibody (CC2), whereas GAPDH was detected by a specific antibody and served as a control. Molecular size markers are shown on the right. (c) Western blotting of CADM1 in SCLC cells with (left) or without (right) *N*-glycosidase treatment.

expressing a high amount of CADM1, were treated with PNGase F and examined by Western blotting. The molecular weight of CADM1 protein was greatly reduced after treatment with PNG-F, indicating that CADM1 is modified by *N*-glycosylation, as reported previously,[8] although the degree of N-glycosylation does not correlate with the malignant feature of these 4 cell lines (Fig. 1c). A couple of distinct signals, however, were still recognized in all SCLC cells after the treatment of N-glycosydase. Because four splicing variants of CADM1 corresponding to exons 8–10 were reported previously (Fig. 2a),[29,30] we determined the sequences of CADM1 cDNA corresponding to exons 7–11 by RT-PCR and sequencing. As shown in Fig. 2b, normal human lung cDNA expressed a single major isoform, variant 8, containing the sequences corresponding to exons 7, 8 and 11. In contrast, for normal human brain cDNA, there were three major isoforms, including variant 8(–) containing exons 7 and 11, variant 9/10 containing exons 7, 9, 10 and 11, and a novel variant 9 containing exons 7, 9 and 11. For human brain cDNA, there were three additional isoforms with trace amounts, including variant 8, variant 8/9 containing exons 7, 8, 9 and 11, and another novel variant 8/9/10 containing exons 7, 8, 9, 10 and 11. Notably, all 14 SCLC cells expressing CADM1 contain a significant amount of variant 8/9, as does variant 8 (Fig. 2b,c). In contrast, only a traceable amount of variant 8/9 is detected in 5 NSCLC cells, as is the case in normal human or mouse tissues, except for the testis (Figs. 2b,c and S3). A primary SCLC tumor expresses a significant amount of both variant 8/9 and variant 8 of CADM1, in contrast to 5 other primary NSCLC tumors (Fig. 2d). These findings indicate that the expression of variant 8/9 of CADM1 is specific to SCLC, except for the testis.

Cell aggregation activity and tumorigenicity of small cell lung cancer cells by CADM1. To understand the biological significance of variant 8/9 and variant 8 of CADM1, we obtained SBC5 derivatives expressing significant amounts of variant 8/9 (SBC5-v8/9) and variant 8 (SBC5-v8) and with a control vector (SBC5-c) (Fig. 3a). Immunohistochemical analyses demonstrated that variant 8 and variant 8/9 of CADM1 are expressed at the cell–cell attachment sites and co-localized with F-actin in confluent cells (Fig. 3b,c). In a cell aggregation assay, both SBC5-v8/9 and SBC5-v8 cells formed large aggregates after 60 min of incubation, whereas SBC5-c cells formed fewer aggregates at the same time point (Fig. 4a). The number of particles was significantly reduced in SBC5-v8/9 and SBC5-v8 cells when compared with SBC5-c cells (Fig. 4b). Cell aggregation activity, however, was not essentially changed in the presence or absence of Ca^{2+} and Mg^{2+} in HBSS, suggesting that the aggregation is mediated by CADM1 as one of the Ca^{2+}-independent IgCAM molecules.

We then tested the tumor-forming or suppressing activity of CADM1 variants in SCLC. When 1×10^6 cells of SBC5-v8/9, SBC5-v8 and SBC5-c cells were injected subcutaneously into the back of Balb/c nu/nu mice, SBC5-v8/9 and SBC5-v8 cells developed palpable tumors by 31 days after injection and continued to grow large tumors. By contrast, SBC5-c cells did not form palpable tumors by 70 days after injection (Fig. 4c). These results demonstrate that variant 8/9 and variant 8 of CADM1 promote a tumorigenic phenotype of SCLC.

Suppression of spheroid-like cell growth *in vitro* by RNAi-mediated downregulation of CADM1 in small cell lung cancer. Finally, we suppressed CADM1 expression of NCI-H69 by RNAi and obtained H69/shCADM1 expressing shRNA against CADM1 and H69/shCON expressing control shRNA. Both variant 8/9 and variant 8 of CADM1 were significantly reduced in amount in H69/shCADM1 cells in comparison with H69/shCON cells (Fig. 5a). H69/shCON cells formed large brown spheroids in culture, as did the parental NCI-H69 cells. By contrast, H69/shCADM1 cells formed flatter sheet-like gray aggregation rather than spheroids (shown in Fig. 5b). When we counted the aggregates of more than 10 cells as one particle, large spheroids were observed in 33% of H69/shCON particles, but in only 11% of H69/shCADM1 particles. In contrast, flat sheet-like cell aggregates was observed in only 22% of H69/shCON, but in 34% of H69/shCADM (Table S2). These results